1 **Title:** Crossroads of assembling a moss genome: navigating contaminants and horizontal gene
2 transfer in the moss *Physcomitrellopsis africana*

3 Vidya S. Vuruputoor[1], Andrew Starovoitov[1], Yuqing Cai[2], Yang Liu[2], Nasim Rahmatpour[1],
4 Terry A. Hedderson[3], Nicholas Wilding[4], Jill L. Wegrzyn[1,5]*, Bernard Goffinet[1]*

5 [1]Department of Ecology and Evolutionary Biology, University of Connecticut, Storrs, Connecticut, USA,
6 06269

7 [2]State Key Laboratory of Agricultural Genomics, BGI-Shenzhen, Shenzhen, China; Key Laboratory of
8 Southern Subtropical Plant Diversity, Fairy Lake

9 [3]Bolus Herbarium, Department of Biological Sciences, University of Cape Town, Private Bag, 7701,
10 Rondebosch, South Africa

11 [4]Université de La Réunion, UMR PVBMT, BP 7151, chemin de l'IRAT, 97410 Saint-Pierre, La Réunion,
12 France; Missouri Botanical Garden, P.O. Box 299, St. Louis, MO, 63166-0299, U.S.A.

13 [5]Institute for Systems Genomics, University of Connecticut, Storrs, Connecticut, USA, 06269

14 ORCID numbers:

15 VV: 0000-0002-5836-7054

16 YC: 0009-0009-3715-2482

17 YL: 0000-0002-5942-839X

18 TH: 0000-0002-3537-6599

19 NW: 0000-0003-4029-5387

20 JW:0000-0001-5923-0888

21 BG: 0000-0002-2754-3895

22 * Corresponding authors: Department of Ecology and Evolutionary Biology, University of Connecticut,
23 Storrs, Connecticut, 06269. Email: jill.wegrzyn@uconn.edu and bernard.goffinet@uconn.edu

Running head: *Physcomitrellopsis* genome

Journal: G3 (Genome Report)

Abstract

The first reference genome assembly of the moss *Physcomitrellopsis africana*, a rare narrow endemic terricolous species from southeastern coastal forests of South Africa, is presented here. Phylogenetically, *Physcomitrellopsis africana* bridges the major evo-devo moss models *Physcomitrium patens* and *Funaria hygrometrica*, which diverged from their common ancestor 60-80 million years ago. The *Physcomitrellopsis africana* genome was assembled with both long Nanopore reads (73x) and short Illumina reads (163x). The 440 Mb assembly comprises 2,396 contigs and 23,493 protein-coding genes (BUSCO: C:96.0%[D:13.9%]), including two unique genes of putative microbial origin absent in close relatives. While the informatic approaches to genome assembly are becoming more standardized, best practices for contamination detection are less defined. The long reads sequenced for the *Physcomitrellopsis africana* genome contained approximately 12% contamination originating from microbial sources. This study describes the informatic processes employed to distinguish contaminants from candidate horizontal gene transfer events. Following the assembly and annotation, examination of whole genome duplication, and patterns of gene family expansion and contraction, were conducted. The genome bears signatures of two whole genome duplications shared with *Physcomitrium patens* and *F. hygrometrica*. Comparative analyses of gene family evolution revealed contractions associated with the light harvesting regulatory network in *Physcomitrellopsis africana* in comparison to *Physcomitrium patens* and *F. hygrometrica*. This first high-quality African bryophyte genome provides insights into genome evolution and HGT in an understudied moss lineage.

Keywords: Funariaceae; reference genome; *Physcomitrella*; Bryophyta; HGT; contamination

Article Summary

The first draft genome of the rare moss, *Physcomitrellopsis africana*, endemic to South Africa's southeastern coastal forests, is presented here. The 440 Mb genome fills a critical phylogenetic gap, enabling the first comparative analysis of the genomes of three moss species that diverge over the last 60-80 million years. The analysis uncovered 23,493 genes and provides new insights into genome evolution and gene family expansion/contraction in mosses. Rigorous contaminant filtering also identified two genes uniquely acquired through horizontal gene transfer.

Introduction

Horizontal gene transfer (HGT) is the lateral movement of genetic material between divergent branches of the tree of life. This process is ubiquitous among bacteria, facilitating rapid adaptation through exchange of ecologically important genes (Aminov, 2011). While HGT is less common in eukaryotes compared to prokaryotes, it does play a role in shaping eukaryotic evolution with about 0.04-6.49% of eukaryotic genomes originating from HGT from microbes (Van Etten & Bhattacharya, 2020). During the evolution of land plants, increasing interactions with rhizosphere microbes, particularly bacteria and mycorrhizal fungi, have enabled occasional horizontal transfer of functional genes between these distantly related lineages (Martin et al., 2017). For example, the gene for Killer Protein 4 (KP4) was likely acquired by mosses through HGT from ascomycetes fungi (Guan et al., 2023). Similarly, the HET domain, common in fungal heterokaryon incompatibility genes and involved in self/non-self recognition, was identified as a truncated form in *Physcomitrium patens* (G. Sun et al., 2020). This gene is associated with moss-fungus interactions, possibly as a defense mechanism. Van Etten & Bhattacharya (2020) suggest that rather than merely anecdotal cases, HGT has been an important evolutionary force driving land plant adaptation to new habitats and stressors throughout their evolution.

Accurately detecting the taxonomic origin of genes and confirming horizontal gene transfer (HGT) events is challenging. Many reported cases of HGT in published genomes have proven to be artifacts resulting from contamination that went undetected. For example, the initial analysis of the genome of the tardigrade *Hypsibius dujardini* reported that 17% of its genes originated from HGT (Boothby et al., 2015), a number subsequently revised to only 0.2% of genes (Koutsovoulos et al., 2016). Similarly, claims of novel DNA modifications in mammals

also turned out to be erroneous due to bacterial contamination, highlighting the need for careful analyses and experimental validation (Douvlataniotis et al., 2020). A systematic screening of 43 arthropod genomes by François et al. (2020) revealed extensive bacterial contaminants, often outnumbering true horizontal gene transfer (HGT) events. For example, in the bumblebee *Bombus impatiens*, most contaminating genes were concentrated on just 30 contaminant scaffolds. Based on the size and number of contaminating sequences, it was concluded that the genome of the symbiont *Candidatus Schmidhempelia bombi* was co-assembled with its host. Strategies to confidently identify HGT, including taxonomic assignment of candidates via BLASTp/DIAMOND, phylogenetic analysis with candidate and donor proteins, synteny analysis of flanking genes, and quantitative PCR validation, have been presented to address these issues (Francois et al., 2020).

These strategies have been applied in recent land plants to identify HGT candidates For instance, the genomes of two fern species, *Azolla filiculoides* and *Salvinia cucullata*, were sequenced and screened for HGT by Li et al. (F.-W. Li et al., 2018)). A fern-specific insect resistance gene identified in *A. filiculoides* appears to have originated from bacteria via HGT based on phylogenetic analyses showing clustering of the fern gene with bacterial orthologs. The authors confirmed candidates by analyzing flanking genes and performing RT-PCR. A similar methodology was used in a large analysis of HGT across land plants, comparing candidates to "donor" and "recipient" databases (Ma et al., 2022).

Physcomitrellopsis africana inhabits transitional zones between grassland and forests in coastal habitats in South Africa. It is currently the sole species of the genus, which likely should also include several species of the paraphyletic genus *Entosthodon* (Wilding, 2015). This resource complements those available for *Funaria hygrometrica* and *Physcomitrium patens* (Kirbis et al., 2022; Rensing et al., 2008) and thereby constitutes a fundamental resource to further the reconstruction of the evolution of the genome of *Physcomitrium patens*, which is widely used in comparative genomics and land plant phylogenomics (Rensing et al., 2020). The first genome of an African bryophyte, a 440 Mb reference for the moss, *Physcomitrellopsis africana*, is presented here. Through rigorous contamination screening and verification, two unique candidate HGT events are described from this assembly. Characterizing validated HGT events in *Physcomitrellopsis africana* yields evolutionary insights while underscoring the need for stringent standards to support HGT conclusions from genomics data.

Materials and Methods

Sample collection and culturing

A population of *Physcomitrellopsis africana* was sampled in October 2010 from a coastal forest in the Eastern Cape Province of South Africa (Dwesa National Park, along trail to chalets behind campground, coordinates 32°18.222' S 28°49.666', at ± sea level). The voucher specimens collected by Goffinet (collection numbers 10326 and 10329, with T Hedderson and N Wilding) are deposited in the CONN herbarium under accession numbers CONN00235389 and CONN00235388, respectively. Specimen 10326 (culture and long read library DNA #5074) provided DNA for genome sequencing and assembly, while 10329 (RNA and Illumina DNA #5075) provided RNA and DNA for Illumina sequencing. Sterile cultures were first established on Knop medium using spores from a single operculate capsule. The gametophytes were harvested, ground and spread on a rich sandy loam soil in PlantCon tissue culture containers (MP Biomedicals, Solon, OH, USA), and maintained in a growth chamber under 16 h of daylight at about 24℃.

Genomic DNA and RNA extraction

Gametophytic tissue, stems and leaves, of *Physcomitrellopsis africana* was harvested from fresh soil cultures under a dissecting microscope and ground in liquid nitrogen. DNA was extracted by following a modified protocol by Young LA (2022). The quality of the DNA sample 5074 was assessed by quantitative PCR prior to sequencing, yielding a DIN score of 7.0 and concentration of 40.9 ng/µL. The DNA was then prepared for PromethION sequencing through a DNA repair step, generating blunt ends, and ligating sequencing adapters followed by priming of the flow cell, as described in the Oxford Nanopore Technologies Amplicons by Ligation (SQK-LSK109) protocol.

DNA for short read sequencing was extracted using the NucleoSpin Plant midi DNA extraction kit, following the manufacturer's protocol (Macherey-Nagel, Düren, Germany). DNA quality was evaluated using a Qubit® 3.0 Fluorometer (Thermo Fisher Scientific, USA). Total RNA was extracted from approximately 1 g of fresh gametophytic tissue using the RNeasy Plant Mini Kit (Qiagen, Valencia, CA, USA).

Genome and transcriptome library preparation and sequencing

The HMW DNA library was sequenced on the Oxford Nanopore PromethION long-read sequencing instrument. The short-read DNA libraries were sequenced (150 bp PE) on two lanes of a BGISEQ-500 sequencing platform (BGI-Shenzhen, China), library preparation followed the methods used by Yu et al (2020).

Approximately 1 µg of RNA was used to generate two paired-end libraries with an insert fragment size of 200–300 bp of the corresponding cDNA. RNA purification, reverse transcription, library construction and sequencing were performed at WuXi NextCode (Shanghai, China). The captured coding regions of the transcriptome from total RNA were prepared using the TruSeq® RNA Exome Library Preparation Kit. The two RNA libraries were sequenced on one lane of an Illumina HiSeq 2000 instrument (100 bp PE) at the WuXi NextCode (Shanghai, China).

Quality control of genomic and transcriptomic reads

The genomic short reads were first assessed with FASTQC v.0.11.7 (Andrews, 2010). In preparation for assembly with Haslr and Wengan, Sickle v.1.33 with a minimum quality score threshold of 30 (-q) and a minimum length of 50 bp (-l) was employed for reads trimming. Nanoplot v.1.21.0 was used to quantify and assess the quality of the Oxford Nanopore PromethION long-read sequences. To detect potential contamination, the long reads were aligned against the provided bacterial, human and viral databases with Centrifuge v.1.0.4-beta (p+h+v; min-hit length was increased to 50 bp) (Kim et al., 2016). Reads aligning to the target loci in the databases were removed. The quality of the transcriptomic short reads was assessed with FASTQC v.0.11.7 (Andrews, 2010). The reads were trimmed with Sickle v1.33 (Joshi NA, 2011) with a minimum quality score threshold of 30 (-q) and a minimum length of 40 bp (-l).

Genome size estimation

A single lane of Illumina short-read genomic data from accession 5075 was employed to estimate the genome size. The k-mer distribution was calculated using Jellyfish v2.2.6 (Marçais & Kingsford, 2011) and size estimates were processed with GenomeScope v2.0 (Ranallo-Benavidez et al., 2020; Fig. S1).

Transcriptome assembly

The transcriptome was independently assembled to provide protein-level evidence for the structural annotation of the genome, using Trinity v2.6.6 (Grabherr et al., 2011), with a minimum contig length of 300bp. Contigs with minimal read support, post assembly, were removed (FPKM > 0.5) with RSEM v1.3.0 (B. Li & Dewey, 2011). Transdecoder v3.0.1 (Haas et al., 2016) was used to translate the remaining contigs into Open Reading Frames (ORFs) and remove sequences without a viable frame. To aid Transdecoder in the identification of ORFs, searches against the Pfam database were performed with HMMER v3.1b2 (Z. Zhang & Wood, 2003). Transdecoder annotated the putative transcripts as complete, partial, and internal. Those without a defined start and stop codon (defined as internals) were removed (split_frames.py). The final set of peptide sequences were functionally annotated with EnTAP v0.8.0 (Hart et al., 2020) against NCBI's nr protein database and the UniProt/Swiss-prot reference databases. EnTAP was run with contaminant filters that included bacteria, archaea, fungi, and insecta. Transcripts with high confidence alignments to these organisms were removed (contam_removal.py).

Genome assembly

Hybrid genome assembly, integrating both long and short-read data, was conducted with MaSuRCA v.4.0.3 (Zimin et al., 2013), Wengan v.0.2 (Di Genova et al., 2021), and Haslr v.0.8a1 (Haghshenas et al., 2020). Additionally, a separate assembly using only long-reads as input was conducted with Flye v.2.5 (with three polishing iterations) (Kolmogorov et al., 2019).

The Flye, Wengan, and Haslr assemblies were polished following long-read alignment with Medaka v1.3.2 (github.com/nanoporetech/medaka). Post assembly with Wengan, the assembly was filtered to remove scaffolds less than 3 Kb. To further improve the accuracy of the assemblies, the hybrid assembly generated by MaSuRCA was polished with the Illumina short reads using Pilon v.1.24 (Walker et al., 2014). Subsequently, the selected MaSuRCA assembly was processed with Purge Haplotigs v.1.0 (Roach et al., 2018).

The Purge Haplotigs pipeline categorized the assembled scaffolds into four coverage levels based on the distribution of mapped reads. This categorization enabled the identification and removal of redundant sequences exhibiting low coverage, presumed to represent erroneous duplicates given the haploid genome. Specific cutoff values of 0, 7, and 65 for the coverage levels were selected to delineate scaffolds to be retained or discarded, based on the k-mer coverage distribution peaks (Fig. S2). The term "allele" is used to describe these redundant

sequences for convenience, although technically inaccurate for a haploid genome. The coverage analysis and purging allowed isolation of the primary genome sequence from duplications and artifacts generated during assembly.

To evaluate the quality of the assemblies, QUAST v5.2.0 (Gurevich et al., 2013) and BUSCO v4.1.2 (viridiplantae_odb10) (Manni et al., 2021) were employed. Each assembly was also evaluated with Merqury v1.3 (Rhie et al., 2020).

Structural and functional genome annotation

Repeat library construction and masking

The repeat library for the final MaSuRCA assembly was generated using RepeatModeler v.2.01 (Flynn et al., 2020) with the long terminal repeat (LTR) discovery pipeline enabled. The genome was then soft-masked with RepeatMasker v.4.0.9-p2 using the consensus repeat library from RepeatModeler (Smit, AFA, Hubley, R & Green, P., 2013-2015).

Structural and functional genome annotation

The Illumina RNA reads were aligned to the soft-masked MaSuRCA assembly with HISAT2 v.2.1.0 (Kim et al., 2019) to provide evidence for protein-coding gene prediction. Two gene prediction analyses were run on the soft-masked assembly using BRAKER v.2.1.5 (Brůna et al., 2021), one with RNA-Seq alignment evidence and one with protein evidence originating from *de novo* assembled transcriptome. Gene predictions from both BRAKER runs were integrated with TSEBRA v.1.0.3 (Gabriel et al., 2021). From this point, separate assessments were conducted on the RNA-Seq evidence gene predictions (BRAKER) and the final TSEBRA gene predictions to select the best approach. Putative genes were removed from both sets if they did not contain a complete protein domain. This filter was applied with Interproscan v.5.35-74.0 (Jones et al., 2014) using the Pfam database v32.0 (Finn et al., 2014). It is worth noting that mono-exonic genes can be the result of fragmented annotations and the target metric of 0.2 (mono:multi-exon gene ratio) is often achieved through protein domain filters (Vuruputoor et al., 2022). Metrics for the gene predictions were generated with gFACs v1.1.3 (Caballero & Wegrzyn, 2019) and BUSCO. After assessment, the filtered BRAKER gene predictions were selected for functional annotation with EnTAP v.0.10.8 (Hart et al., 2020). Functional annotation reports from EnTAP

(both sequence similarity search and EggNog taxonomy scope classifications) allowed for the identification of non-target species scaffolds in the assembly (Huerta-Cepas et al., 2019).

Assembly level contaminant filtering

Using the functional annotation results from EnTAP, contaminated scaffolds were removed. Scaffolds with a length of 10 Kb or less, and with 40% or more of their total genes classified as archaea, bacteria, or fungi, were removed. Additionally, scaffolds greater than or equal to 10 Kb with 55% or more genes classified as archaea, bacteria, or fungi, were also excluded. The final annotation was then assessed for the annotation rate using EnTAP, the mono:multi ratio using gFACs, and BUSCO completeness.

Horizontal gene transfer candidate identification

To identify candidate HGTs in *Physcomitrellopsis africana*, protein sequence similarity searches were conducted with Diamond v2.1.8 (Buchfink et al., 2021). The protein sequences of *Physcomitrellopsis africana* were aligned against "donor" databases, which included sequences from bacteria, fungi, archaea, and metazoa from NCBI's nr database. Additionally, the same proteins were aligned to "recipient" databases containing sequences from Streptophyta, Tracheophyta, Embryophyta, Viridiplantae, and Spermatophyta (Ma et al., 2022). Although these categories are not fully exclusive, each database was utilized separately to systematically assess presence across plants at different evolutionary divergence points.

To identify candidate genes representing putative horizontal gene transfer (HGT) events unique to *Physcomitrellopsis africana*, the following criteria were utilized: genes were required to have between one and four significant sequence alignments (E-value <1e-5) to microbial donor databases, while exhibiting no significant sequence similarity to plant recipient databases. This range of one to four microbial alignments was selected to capture potential HGTs while avoiding ubiquitous domains shared across many microbes. The lack of hits to plant databases was intended to enrich for *Physcomitrellopsis africana*-specific sequences, rather than those conserved across plants through vertical inheritance. At this stage, any scaffolds containing only bacterial or fungal genes, without any plant-related genes, were removed from the assembly.

To assess the validity of the two proposed HGT candidates, the genes were visualized on the

Integrated Genome Viewer (IGV). The alignments of the HGT candidates from the 'nr' database, as well as the transcripts assembled with StringTie2 (Kovaka et al., 2019), were visualized.

Analyzing HGT candidates from Physcomitrium patens

The 264 putative horizontally transferred genes (HGTs) previously identified in *Physcomitrium patens* (J. Zhang et al., 2020) were independently searched against the *Physcomitrellopsis africana* and *F. hygrometrica* protein sets using DIAMOND v2.1.8 (Buchfink et al. 2021). DIAMOND searches were conducted with an E-value cutoff of 1e-5 and max target sequences set to 1. Hits against *Physcomitrellopsis africana* and *F. hygrometrica* were collected and merged to generate a summary table with *Physcomitrium patens* HGTs and the respective top hits in each species.

Comparative genome analyses

A comparative analysis of the protein-coding gene space was conducted with OrthoFinder v.2.5.1 (Emms & Kelly, 2019) with *F. hygrometrica* (Kirbis et al., 2022) and *Physcomitrium patens* v3 (Lang et al., 2018). To provide a preliminary estimate of gene family size dynamics, gene counts from each species in the assembled orthogroups were categorized as neutral, expanded, or contracted. The first and third quartiles were calculated for the distinct gene counts within a gene family for each species. If the number of genes from a species was lower than the first quartile or higher than the third quartile, then the gene family was categorized as "contracted" or "expanded", respectively. If the number of genes did not fit with either of these two criteria, then the gene family was considered "neutral". The longest gene for each orthogroup was used to assign functional attributes to all genes in the group from the original EnTAP annotation. If the longest gene did not originate from *Physcomitrellopsis africana*, then the functional annotation was derived from either *Physcomitrium patens* or *F. hygrometrica*.

GOSeq (Young et al., 2010) enrichment analysis was performed in R v4.2.0. GO terms were extracted for each gene from the EnTAP run. Enrichment analysis was investigated separately for *Biological Process* and *Molecular Function* GO categories. Paralogs of LHC, STN7, and STN8 were identified with Diamond v2.8.1 (E-value <1e-5).

Whole genome duplication analysis

Chromosome-scale genomes of *F. hygrometrica* and *Physcomitrium patens* were assessed with the reference genome generated for *Physcomitrellopsis africana,* with wgd (v.1.0.1) to characterize whole genome duplication events (Zwaenepoel & Van de Peer, 2018). Each species was compared against itself. Nucleotide sequences (CDS) were used as input to Blast & Markov clustering (MCL) (Altschul et al., 1997; van Dongen, 2000). A Ks distribution was constructed using the 'ksd' subcommand and 'mcl' output (Katoh & Toh, 2008; Price et al., 2010; Yang, 2007). Next, a collinearity analysis was performed with 'syn' using the structural genome annotations (Proost et al., 2011). Gaussian mixture models, via 'mix', were used to generate Ks distributions to aid in component interpretation. Model fit was evaluated with the Bayesian and Akaike information criterion (BIC/AIC).

Results and Discussion

Sequencing and quality control of genomic reads

The single ONT PromethION run generated 16 million reads (N50: 7,518 bp; 127X coverage: 404 Mb; 116X coverage: 440 Mb; Table S1). Centrifuge filtering reduced this set to approximately 14M reads (N50: 4,561 bp; 80X coverage: 404 Mb; 73X coverage: 440 Mb). The primary contaminants included bacteria from *Xanthomonadaceae* (10.68%) followed by *Bradyrhizobiaceae* (0.7%). The BGISEQ-500 short-read genomic libraries (100 bp PE) generated 529 M reads. Following trimming with Sickle, 360 M reads remained (178X coverage: 404 Mb; 162X coverage: 440 Mb; Table S2). Coverage estimates are provided for both the original estimate (404 Mb) and the final assembled genome size (440 Mb).

Transcriptome assembly

A total of 36.58M Illumina short reads were generated. Following quality filtering using Trimmomatic, the dataset was reduced to 31.84M reads. The *de novo* assembly process with Trinity yielded 143,150 contigs. After expression filtering via RSEM, the number of contigs was reduced to 123,373. Identifying open reading frames (ORFs) in the contigs resulted in 110,852 successfully translated transcripts. The average sequence length of these translated ORFs was 803 bp, with an N50 value of 1,038 bp. To enhance the quality of the transcriptome assembly,

internal sequences and putative contaminants were removed, resulting in 74,997 total transcripts. After removing internal sequences and contamination, the total unique sequences with an alignment is 51,982 (69.3%; File S1). The final BUSCO score of the remaining transcripts was C:82%[D:35.7%]. A total of 30,657 (36.6%) transcripts aligned to *Physcomitrium patens* proteins. An assessment of contamination revealed 8,720 (10.41%) of sequences potentially contaminated, with contributions from various sources such as amoeba (0.40%), bacteria (3.8%), fungi (94.99%), and insecta (0.77%). A total of 15,500 (18.5%) sequences remained unannotated.

Genome assembly

Initial assembly: Multiple genome assembly approaches were employed to generate comprehensive draft assemblies of the *Physcomitrellopsis africana* genome (Fig. 2). The long-read approach, Flye, assembled 538.68 Mb in 8,388 scaffolds, with an N50 of 152.58 Kb. The BUSCO completeness score was C:84.0%[D:12.2%] and the Merqury QV score was 21.1. Among the hybrid approaches, Haslr produced a 295.98 Mb reference distributed across 12,738 scaffolds, with an N50 of 52.29 Kb. The BUSCO score was C:94.1%[D:13.2%], and the QV score was 11.9. Wengan assembled a total of 466.64 Mb across 10,516 scaffolds, with an N50 of 119.42 Kb and a BUSCO score of C:96.4%[D:18.8%], and a QV score of 27.4. Finally, MaSuRCA assembled 506.22 Mb across 3,571 scaffolds, with an N50 of 381.33 Kb, (BUSCO: C:96.4%[15.5%], and a QV score of 31.0).

Polishing and improving genome assembly:

The Medaka polished Flye assembly had a genome size of 530.57 Mb in 8,386 scaffolds, and the N50 was decreased to 145.17 Kb. The BUSCO dropped to C:90:3%[D:11.5%]. The QV score decreased to 19.6. Polishing of the Haslr assembly resulted in a genome size of 295.73 Mb, across 12,737 scaffolds. The N50 remained almost unchanged at 52.31 Kb, and the BUSCO score reduced to C:90.6%[D:9.4%]. The QV score more than doubled to 25.2. Filtering for scaffolds less than 3 Kb, followed by Medaka, resulted in a smaller genome size for the Wengan assembly at 434.41 Mb across 7,639 scaffolds. The N50 increased to 132.40 Kb. The BUSCO score was reduced to C:93.2%[D:11.8%], and the QV increased slightly to 27.5.

Polishing with Pilon had very minimal little influence on the completeness, as expected, and substantial impact on the accuracy of the MaSuRCA assembly. The polished MaSuRCA

hybrid assembly size increased slightly to 507.10 Mb across 3,590 scaffolds, with a slightly decreased N50 of 378.43 Kb. The BUSCO completeness remained the same at C:96.4%[D:15.5%], and the QV score increased to 35.6.

Refinement of genome assemblies with Purge-haplotigs: The MaSuRCA assembly was selected for further refinement. This decision was based on the overall quality assessed by Merqury, BUSCO completeness, and overall contiguity. The MaSuRCA assembly was refined with Purge-haplotigs which reduced the assembly length to 502.34 Mb across 3,237 scaffolds with an N50 value of 382.25 Kb. The BUSCO completeness score remained the same (e.g., 96.4%) and the QV score was minimally reduced to 35.5. At 502.34 Mb, the assembled genome is ~100 Mb longer than the k-mer based estimate (440 Mb, Fig S1).

Genome annotation

Repeat identification: RepeatModeler produced a library containing 580 unique repeats that were used to softmask 50.22% of the final assembly (Table S3; File S2). Of the repeats, 36.53% was composed of *Ty3/Gypsy* and 1.46% of *Ty1/Copia*. This is similar to the pattern in *Physcomitrium patens*, wherein approximately 57% of the genome is composed of repeat elements, with long terminal repeats (LTRs), particularly the *Gypsy* family, accounting for 48% of the masked genome (Lang et al., 2018). These findings align with observations by Kirbis et al. (2022), suggesting a common pattern across these species regarding the activation of *Gypsy* elements in *Physcomitrellopsis africana* and *Physcomitrium patens*. In contrast, *F. hygrometrica*, which diverged from *Physcomitrium patens* 60 to 80 MYA (Bechteler, Peñaloza-Bojacá, Bell, Burleigh, McDaniel, et al., 2023; Medina et al., 2018), exhibits a lower overall repeat estimate of 35%. Here, *Gypsy* elements contribute less to the LTR content, i.e., roughly 10%, whereas *Copia* elements contribute 17%.

Protein-coding gene identification: The *Physcomitrellopsis africana* RNA-Seq reads had an overall alignment rate of 78.43%, likely due to contaminant content, but a substantial set of 37M reads were retained, exceeding the minimum needed for prediction. The first BRAKER2 predictions, using RNA-Seq evidence alone, generated 60,917 protein-coding genes with a BUSCO completeness score of C:95.8%[D:15.3]. The mono:multi exonic ratio was 0.52. With only protein evidence, BRAKER2 generated 37,752 gene predictions with a BUSCO score of

C:46.1%[D:16.0]. Merging these predictions, as recommended by TSEBRA, resulted in a set of 45,737 genes with a BUSCO score of C:91.3%[D:15.1], and the mono:multi exonic ratio was 1.06. The gene prediction set generated with RNA-Seq alignment evidence exclusively was selected for further refinement due to its higher BUSCO score and lower mono:multi ratio compared to the merged TSEBRA transcripts. Through protein domain filtering (InterProScan filter), the number of mono-exonic genes was further reduced from 20,081 to 12,696, producing a total of 23,561 genes (BUSCO: C:93.8%[D:13.8%]; mono:multi ratio: 0.08).

A total of 831 scaffolds, a total of 1250 genes associated with contaminants were removed, based on the functional annotations of the gene space. This also reduced the assembly length to 440 Mb in 2,406 scaffolds with an N50 of 363 Kb, and an assembly BUSCO score of C:96%[D:13.9%]. This substantial reduction led to an assembly within ~40 Mb of the original k-mer-based estimate (e.g., 404 Mb).

The annotated protein-coding gene space in the contaminant-filtered assembly included 1,708 mono-exonic and 21,853 multi-exonic genes. The annotated gene space has a BUSCO score of C:93.8%[D:13.6%], with a mono:multi ratio of 0.08. Reciprocal BLAST conducted by EnTAP produced an annotation rate of 78%, of which 93.6% aligned to *Physcomitrium patens* (Table 1; File S3). This contrasts with the annotation rate of 50% in *F. hygrometrica* (Kirbis et al., 2022), likely attributed to significant divergence time from the model *Physcomitrium patens,* and the lack of closely related species in public genomic databases (Kirbis et al., 2020; Rahmatpour et al., 2021). The higher annotation rate in this study suggests that many genes found in *Physcomitrium patens* but not *F. hygrometrica* may have been acquired in the ancestor of the *Physcomitrellopsis-Entosthodon-Physcomitrium* clade (Medina et al., 2019).

Comparative genome analysis

In comparison of the three genomes of *Physcomitrellopsis africana*, *F. hygrometrica*, and *Physcomitrium patens*, a total of 14.2K orthogroups are shared among the species, and 959, 936, and 179 are, respectively, unique to each species. *F. hygrometrica* and *Physcomitrellopsis africana* exclusively share more (1092) orthogroups than *Physcomitrellopsis africana* and *Physcomitrium patens* (809) (Fig. 3A), despite the latter sharing a more recent unique common ancestor (Fig. 1). Thus, whereas Funariaceae share a rather conserved architecture of their

vegetative body even after at least 60 MY of divergence, their gene space varies considerably, reflecting significant innovation (Kirbis et al. 2022) perhaps driven by ecophysiological adaptations (Glime, 1990). Of the putative gene families from the *Physcomitrellopsis africana* annotation, 809 and 1,694, respectively, were categorized as expanded and contracted (File S4). Enrichment analysis examined through Gene Ontology's *Biological Process* category revealed 167 expanded terms and 6 contracted terms. In contrast, within the *Molecular Function* GO category, 62 were contracted, and no terms were significantly expanded.

Although expanded *Biological Process* GO terms were excessively broad, orthogroup analysis revealed a pattern of contraction in GO terms pertaining to oxidoreductase activity, FMN binding, and serine protease activity (Fig. 3B). Whether this unique suite of downregulated categories diagnoses photosynthetic properties of *Physcomitrella africana* only or of the expanded genus sensu Wilding (2015) remains to be tested.

The complement of light-harvesting complex (LHC) genes are expanded in the moss *Physcomitrium patens* compared to algae and vascular plants (Alboresi et al., 2008; Iwai et al., 2018). LHC proteins bind chlorophylls and carotenoids to facilitate light absorption and energy transfer to the reaction centers of Photosystems I and II. The LHC genes are classified into two groups: Lhca encodes antenna proteins for PSI (LHCI) while Lhcb encodes antenna proteins for PSII (LHCII). Although ancestral land plants contain several LHC homologs, further expansion and redundancy occurred in *Physcomitrium patens* after whole genome duplication events (Alboresi et al., 2008; Rensing et al., 2008; H. Sun et al., 2023; Zimmer et al., 2013). This led to a larger repertoire of LHC genes compared to the alga *Chlamydomonas reinhardtii* and the vascular plant *Arabidopsis thaliana*. Specific Lhca and Lhcb paralogs are represented in multiple copies in *Physcomitrium patens* compared to one to two copies in the other species. The major antenna proteins encoded by Lhcbm also show greater redundancy and diversity in *Physcomitrium patens* (Iwai et al., 2018; H. Sun et al., 2023).

Comparing the genomes of *F. hygrometrica* and *Physcomitrellopsis africana* to the reference genome of *Physcomitrium patens* reveals both conservation and divergence of LHC genes. For example, while *Physcomitrium patens* has 12 distinct Lhca compared to 8 distinct Lhca in *Physcomitrellopsis africana*, and 7 distinct Lhca in *F. hygrometrica*. Similarly, while *Physcomitrium patens* has 12 distinct Lhcb, *Physcomitrellopsis africana* has 8, and *F.*

hygrometrica has 9. Finally, *Physcomitrium patens* has 14 distinct Lhcbm, *Physcomitrellopsis africana* has 2, and *F. hygrometrica* has 8. Two rounds of whole genome duplication (WGD) occurred in the most recent common ancestor of the Funariaceae, as evidenced by shared duplication signatures across all three genomes (Fig. S3). However, echoing Kirbis et al. (2022), more duplicates from these WGDs were retained in *Physcomitrium patens* than in *F. hygrometrica* and *Physcomitrellopsis africana*. Whereas *Physcomitrium patens* retained multiple LHC paralogs as a result of the ancestral WGDs, *F. hygrometrica* and *Physcomitrellopsis africana* seem to have lost some of this redundancy. This pattern of differential retention is further supported by assessing the number of paralogs and orthologs for each LHC gene family across the three genomes (Table S4). Although some copies of LHC genes were lost in *F. hygrometrica* and *Physcomitrellopsis africana*, key STN7 and STN8 kinases involved in photosynthetic acclimation are conserved and retained in all three genomes, suggesting retention of core light signaling components.

Contaminant filtering and the identification of horizontal gene transfer events:

Horizontal gene transfer (HGT) involves the exchange of genetic material between different organisms, extending beyond prokaryotes, with instances observed within eukaryotes as well (Guo et al., 2023; Kirsch et al., 2022; Xi et al., 2012). While lateral transfer can occur between related plant lineages through hybridization, HGT in mosses involves exchange between evolutionarily distant microbes and land plants. Mosses, which originated 500 million years ago (Bechteler, Peñaloza-Bojacá, Bell, Burleigh, Mcdaniel, et al., 2023), have formed symbiotic relationships with microbes, aiding in nutrient acquisition and stress resistance (Berg et al., 2016; Hornschuh et al., 2006). In addition, genes of putative fungal origin regulate developmental transitions in mosses (Wang et al., 2020).

Several reports of HGT in eukaryotes were later reclassified as contamination. The assembly of *Physcomitrellopsis africana* employed filtering processes before and after genome assembly, illustrating that comprehensive approaches at all stages significantly enhanced the final genome assembly. Here, metagenomic tools optimized for long-reads identified contaminants prior to assembly. Since this initial filter did not include the short reads or assess fungal contributions in either sequence set, further filtering was conducted after assembly and annotation. The protein-coding genes were functionally characterized through sequence

similarity. An estimated 22% of the genes were of fungal origin and 31% were of bacterial origin. Scaffolds that contained a majority of genes likely originating from algae, bacteria, or fungi (ABF) were removed. Separately, the annotated gene space was aligned to a set of "donor" and "recipient" databases. This identified 31 potential horizontal gene transfer (HGT) events. Following the set of best practices outlined by François et al. (2020), an additional set of 10 scaffolds were found to be contaminated as the flanking genes of the potential HGT candidates were not of plant origin. This resulted in their removal (HGT filter). Two unique HGT candidates survived these filters (Fig. 4).

The first HGT candidate, *Pa1_22336.1* (alignment to *Paracoccaceae bacterium*), contains a methyltransferase domain. A recent phylogenetic analysis conducted among bryophytes revealed that DNA methyltransferases identified in *Marchantia polymorpha*, *Physcomitrium patens*, and *Anthoceros angustus* form clades with their bacterial homologs. This suggests that these genes were likely acquired via horizontal gene transfer (HGT) from bacteria (J. Zhang et al., 2020). The second HGT candidate, *Pa1_04828* (alignment to *Pedobacter sp.* SYSU D00873), encodes a glycosyl hydrolase, functioning as an antibacterial defense. This gene family is widely distributed across various taxonomic groups as a result of independent transfers from bacteria to plants, fungi, animals, and archaea. In the hornwort *Anthoceros angustus*, the HGT-derived glycosyl hydrolases are thought to enhance the metabolic adaptability in response to changing environments, particularly in cell wall synthesis and modification (Haimlich et al., 2022; J. Zhang et al., 2020).

These two candidates were manually assessed comparing alignments of *de novo* assembled transcriptomes. *Pa1_22336.1* had transcriptomic support, tentatively increasing confidence in it being a high-confidence HGT event. *Pa1_04828* lacked this transcriptomic support. Both candidates are directly flanked by well annotated plant (moss) genes. Additionally, aligning the full set of *Physcomitrium patens* and *Ceratodon purpureus* proteins to the *Physcomitrellopsis africana* scaffolds produced no alignments in proximity to the candidates, further suggesting that the HGT candidates may be specific to *Physcomitrellopsis africana* (Fig. 5).

Analyzing HGT candidates from Physcomitrium patens: The genomes of *Physcomitrellopsis africana* and *F. hygrometrica* were screened for the 264 putative horizontally transferred genes

(HGTs) previously identified in *Physcomitrium patens* (Ma et al., 2022). Ninety of these genes (34%) were not found in either species,16 (6%) were found in *Physcomitrellopsis africana* and *Physcomitrium patens*, and 7 (3%) were shared between *Physcomitrium patens* and *Funaria hygrometrica*. The greater number of shared HGTs between *Physcomitrium patens* and *Physcomitrellopsis africana* likely reflect their more recent divergence (at least 20 MYA) compared to that of *Physcomitrium patens* and *Funaria hygrometrica* (at least 60 MYA (Bechteler, Peñaloza-Bojacá, Bell, Burleigh, McDaniel, et al., 2023; Medina et al., 2018) (Fig. S4).

Data availability

All scripts and data used are available through https://gitlab.com/PlantGenomicsLab/physcomitrellopsis-africana-genome. Illumina short and Nanopore long genomic reads, RNA-Seq reads, de novo assembled transcripts, whole genome shotgun assembly, and annotation files will be uploaded to NCBI BioProject: PRJNA1020579.

Acknowledgements

The authors would like to thank the Institute for Systems Genomics (ISG) and Computational Biology Core at the University of Connecticut for high-performance computing services.

Funding

This study was made possible through the US National Foundation grants DEB-0919284 (fieldwork), DEB-1753811 to BG, and DBI-1943371 to JW.

Conflict of interest

The authors declare no conflict of interest.

Author contributions

J.W. & B.G. designed the study. B.G., N.W. & T.H. conducted fieldwork to sample the wild population. Y. C. & Y. L. generated genomic and transcriptomic data. A.S. & V.S.V. conducted all analyses. V.S.V., J.W. & B.G. wrote the paper. All authors approved of the final version.

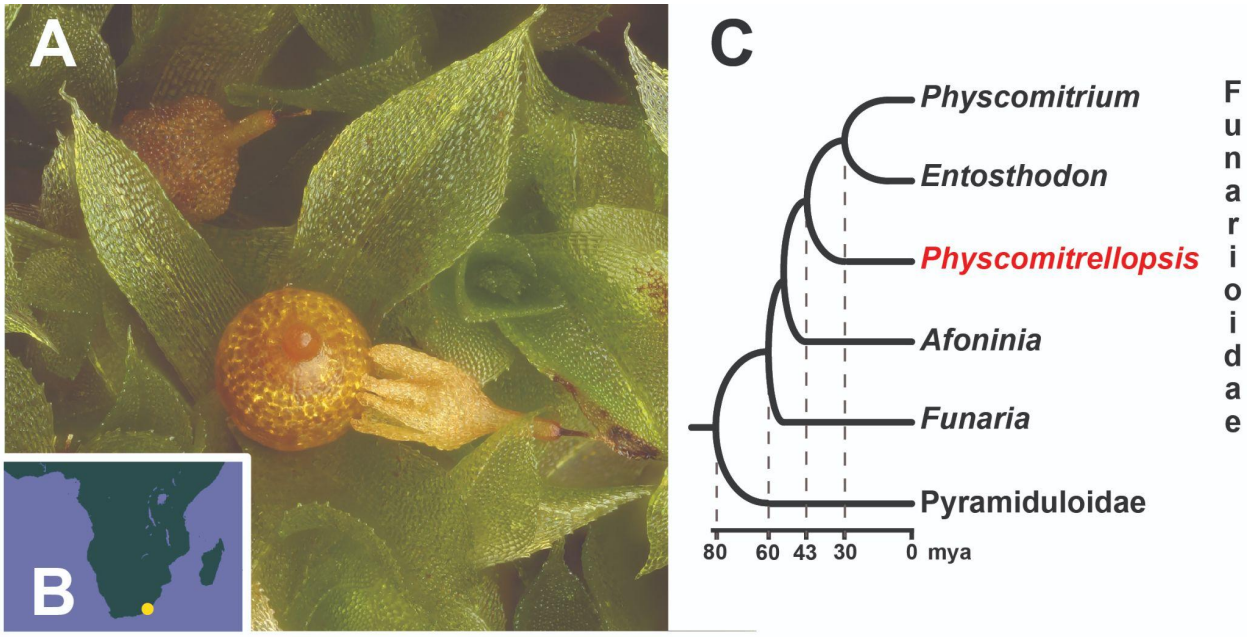

Fig. 1. A *Physcomitrellopsis africana* exhibits a reduced architectural complexity of the sporophyte similar to that observed in *Physcomitrium patens*, namely a sessile, aperistomate and cleistocarpous sporangial capsule. **B** The known geographic distribution of *Physcomitrellopsis africana*, a rare narrow endemic to the Eastern Cape Region in South Africa. **C** Phylogenetic relationships and chronology of the evolution of *Physcomitrellopsis* based on Medina et al. (2018).

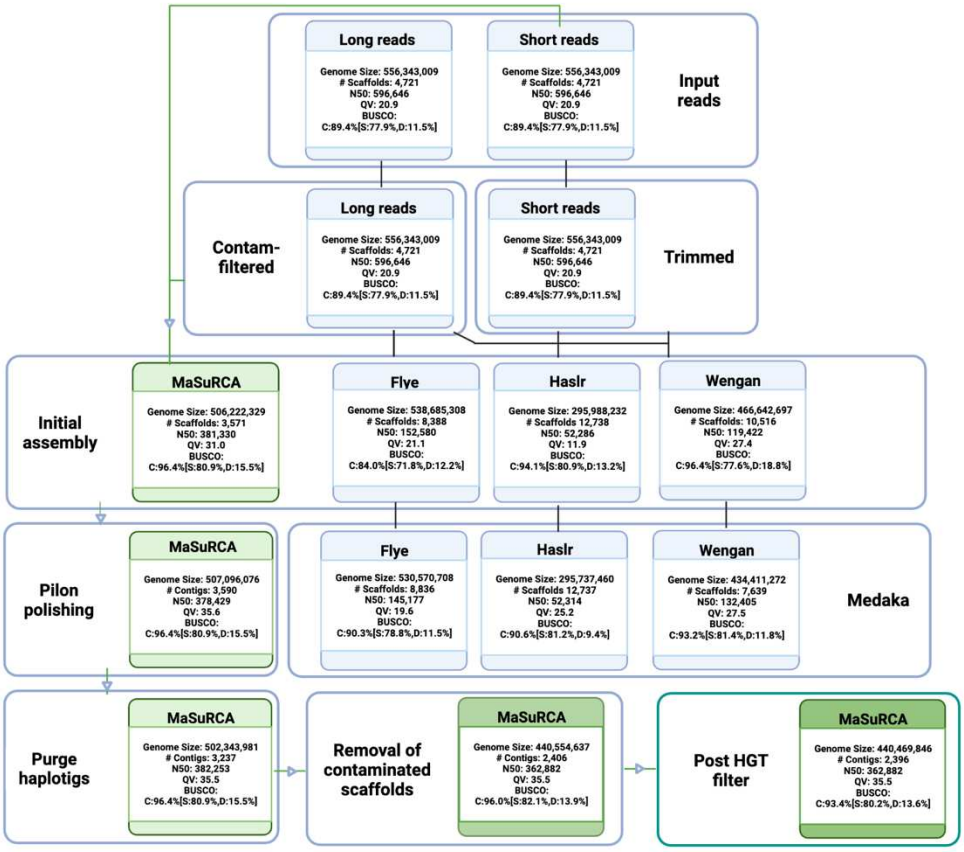

Fig. 2. Workflow and statistics for read QC, genome assembly, polishing, and haplotype phasing. Short reads generated from BGI-seq were subject to trimming and the long reads (ONT) were filtered for contaminants with Centrifuge. Filtered and trimmed reads were utilized as input for four different genome assembly software tools: Flye (long-read only), Haslr, Wengan, and MaSuRCA. The green box indicates the selection of the MaSuRCA assembly for further analysis. The final assembly was polished using Pilon and phased with Purge haplotigs. A total of 831 scaffolds were removed as a result of contaminant filtering using EnTAP following structural genome annotation. Ten additional scaffolds were removed after HGT candidate assessment. Summary statistics derived from Quast, BUSCO, and Merqury are displayed for each process.

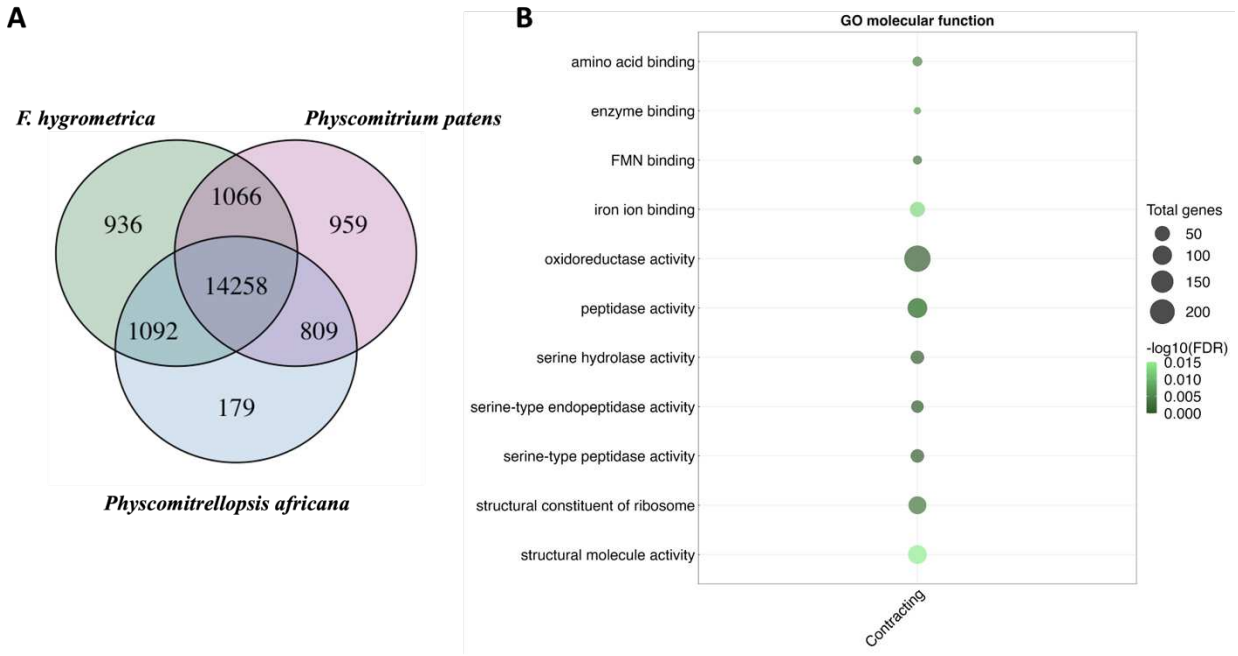

Fig. 3. A Number of shared and unique orthogroups among *F. hygrometrica*, *Physcomitrellopsis africana*, and *Physcomitrium patens*. **B** Enriched *Molecular Function* GO terms for gene families in a comparative analysis between *Physcomitrellopsis africana*, *Physcomitrium patens*, and *Funaria hygrometrica* showed contraction in the GO terms related to oxidoreductase activity, as well as serine peptidase activity and FMN binding for *Physcomitrellopsis africana*. The size of each bubble represents the number of gene families within an orthogroup, and the gradient of the color denotes the significance level of enrichment- the darker green denotes more significance.

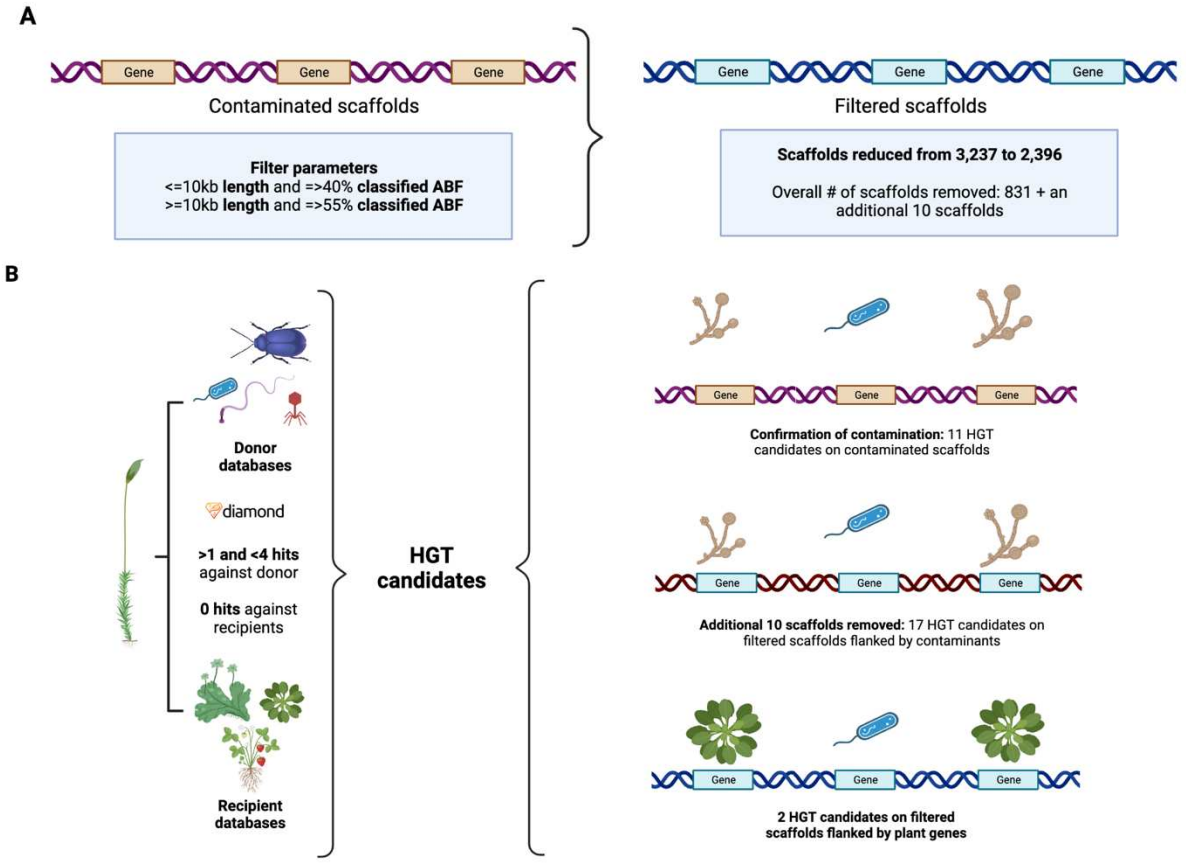

Fig. 4. Contamination versus horizontal gene transfer (HGT) in the *Physcomitrellopsis africana* genome. **A** Parameters used for removing a set of contaminated scaffolds from the draft genome based on functional characterization of the annotated gene space. Scaffolds with a length of 10 kb or less, and those with 40% or more of their total genes classified as archaea, bacteria, or fungi were removed. Additionally, scaffolds with a length greater than or equal to 10 Kb and having 55% or more genes classified as archaea, bacteria, or fungi were also excluded. In total, 831 scaffolds were removed as a result of this filtering process. **B** Identification of HGT candidates via sequence similarity comparisons of *Physcomitrellopsis africana* proteins against both "donor" databases (archaea, bacteria, fungal, and metazoan) and "recipient" databases (Streptophyta, Viridiplantae, Tracheophyta, and Spermatophyta). Proteins with >1 and <4 hits against all of the donor databases, and no hit against recipient databases were labeled as HGT candidates. This analysis was conducted on the contaminated scaffolds removed in A, confirming their contamination status. On the post-filtered scaffolds, there were some putative HGTs that were flanked by contaminants. These scaffolds were also removed from the assembly (additional 10), resulting in the retention of two HGT candidates in the final analysis.

Fig. 5. Integrated Genome Viewer (IGV) screens depicting five tracks of the *Physcomitrellopsis africana* genome. Track 1 shows the protein-coding structural annotation in context to the genome. Track 2 displays genome-guided transcript assemblies via StringTie2. Track 3 illustrates the alignment of the Horizontal Gene Transfer (HGT) candidate (NR database) to the genome. Track 4 and 5 show the alignments of *Physcomitrium patens* and *Ceratodon purpureus* proteins onto the scaffolds 62 and 1363. **A and B** show the HGT candidates *Pa1_04828* and *Pa1_22336.1*, where the HGT candidate alignment validates the presence of a protein, while the StringTie2 transcript does not align with the HGT placement. None of the moss proteins align to the HGT candidates. **C** highlights the example of *Pa1_15636.1,* where the StringTie2 transcript and the MiniProt alignment reveal that the gene spans two gene models, indicating a false identification as an HGT candidate. Further transcriptomic evidence is required to modify the annotation model and establish the validity of these gene models.

572 **Table 1.** Genome annotation statistics for *Physcomitrellopsis africana*

Annotation Method	**Total genes**	**BUSCO (viridiplantae)**	**Mono: multi ratio**	**Annotation rate**
BRAKER (RNA)	60,917	C:95.8%[D:15.3]	0.52	65%
BRAKER (protein)	37,752	C:46.1%[D:16.0]	0.95	73%
TSEBRA (BRAKER RNA + BRAKER protein)	45,737	C:91.3%[D:15.1]	1.02	74%
BRAKER (RNA) + InterProScan filter + scaffold contam filter)	23,561	C:93.8%[D:13.6%]	0.08	78%
BRAKER (RNA) + InterProScan filter + scaffold contam filter + HGT filter)	23,535	C:93.8%[D:13.6%]	0.07	83%

573
574

575 **Table S1.** Pre-QC Read Stats.

Instrument	Total Reads	N50 (bp)	Average Read Length (bp)	Coverage (404 Mb)	Coverage (440 Mb)
Nanopore PromethION	16,640,338	7,518	3,080	127	116
Illumina Genomic Reads	529,496,757	N/A	100 PE	262	240

576

577 **Table S2:** Post-QC Read Stats

578

Read Type	Total Reads	N50 (bp)	Average Read Length (bp)	Coverage (404 Mb)	Coverage (440 Mb)
Nanopore PromethION	14,495,188	4,561	2,233	80	73
Illumina Genomic Reads	359,619,533	N/A	100 PE	178	163

579

580 **Table S3.** Repeat content of the MaSuRCA genome assembly.

Sequences:	3237		
Total Length:	502343981 bp		
GC Level:	36.07%		
Bases Masked:	253596074 bp	50.48%	
	Number of elements	**Length (bp)**	**Percentage of sequence**
Retroelements	182967	203774766	40.56
SINEs	116	50840	0.01
Penelope	44	43124	0.01
LINEs	5635	3528322	0.7
CRE/SLACS	25	87739	0.02
L2/CR1/Rex	0	0	0
R1/LOA/Jockey	0	0	0
R2/R4/NeSL	0	0	0
RTE/Bov-B	0	0	0
L1/CIN4	1520	1352049	0.27
LTR elements	177216	200195604	39.85
BEL/Pao	0	0	0
Ty1/Copia	7771	7313798	1.46
Gypsy/DIRS1	146546	183504589	36.53
Retroviral	0	0	0
DNA transposons	3075	2020920	0.4
hobo-Activator	161	85415	0.02
Tc1-IS630-Pogo	828	502079	0.1
En-Spm	0	0	0
MuDR-IS905	0	0	0
PiggyBac	0	0	0
Tourist/Harbinger	576	270022	0.05
Other	0	0	0
Rolling-circles	7857	3140001	0.63
Unclassified	70182	35763560	7.12
Total interspersed repeats		241559246	48.09
Small RNA	454	382891	0.08
Satellites	0	0	0
Simple repeats	177543	7162961	1.43
Low complexity	26138	1350975	0.27

581

Table S4. Comparison of light-harvesting complex (LHC) gene complements in *Physcomitrellopsis africana*, *Funaria hygrometrica*, *Physcomitrium patens*, *Chlamydomonas reinhardtii**, and *Arabidopsis thaliana** *(Alboresi et al., 2008).* The number of paralogs is shown for key LHC genes including antenna proteins (Lhca, Lhcb) and major light-harvesting proteins (Lhcbm).

Gene	*Physcomitrellopsis*	*Funaria*	*Physcomitrium*	*Chlamydomonas*	*Arabidopsis*
Lhca1	3	2	3	1	1
Lhca2	2	3	4	1	1
Lhca3	2	1	4	1	1
Lhca5	1	1	1	1	1
Lhcbm	2	8	14	9	0
Lhcb3	1	1	1	0	3
Lhcb4	2	2	2	1	4
Lhcb5	2	1	2	1	5
Lhcb6	1	2	2	0	2
Lhcb7	1	1	1	1	1
Lhcb9	1	2	2	9	2

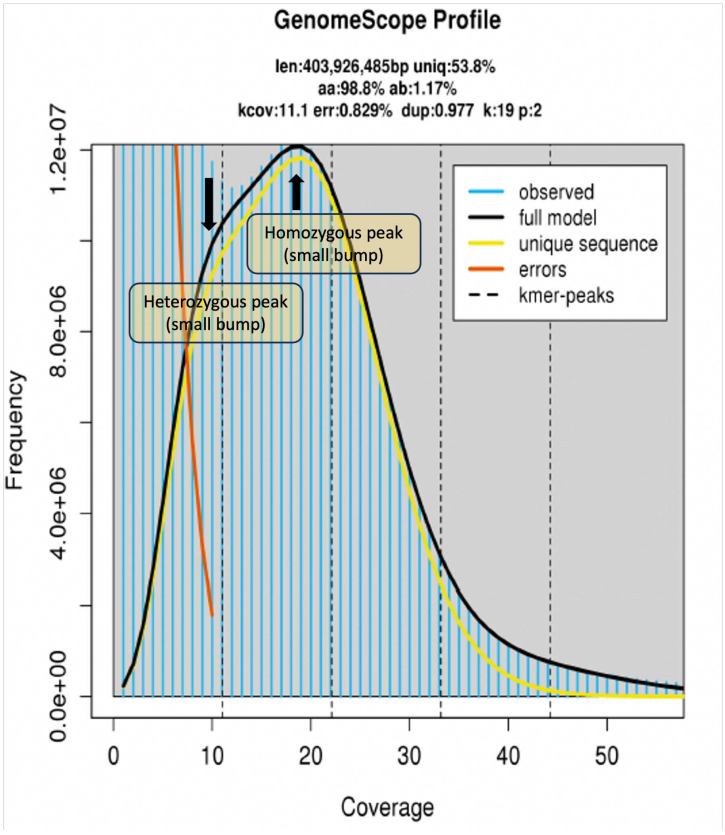

Fig S1: GenomeScope output for preliminary analysis of *Physccomitrellopsis africana*. GenomeScope generates coverage plots to estimate genomic characteristics including len (inferred total genome length), uniq (percent of unique genome), het (heterozygosity rate), kcov (kmer coverage), err (read error rate), and dup (rate of read duplications). The het value of ~1.17% represents a low-end approximation of heterozygosity based on unfiltered short reads. The peak at 9X corresponds to the estimated heterozygous portion (ab) while the peak at 19X corresponds to the estimated homozygous portion (aa). Further data quality control and analyses were performed to reduce heterozygosity, as this is a haploid genome.

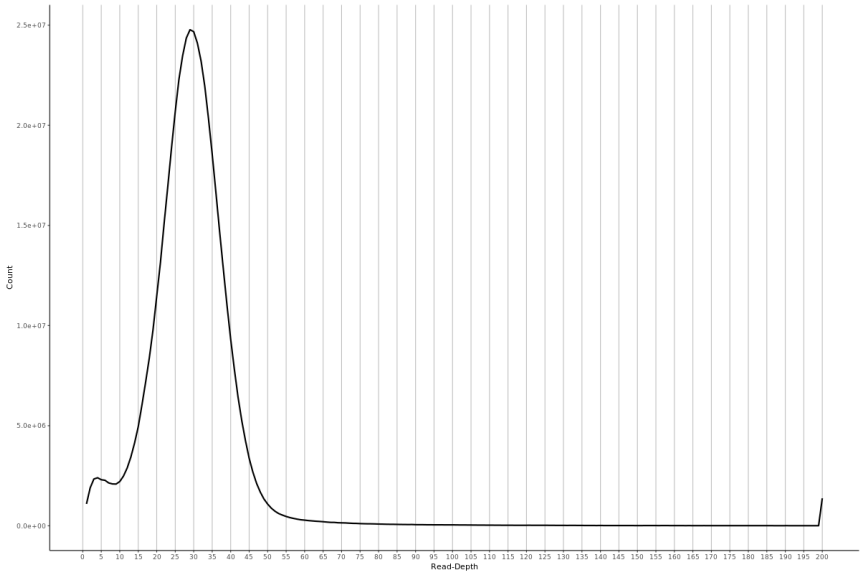

Fig S2: Histogram of k-mer coverage distribution for the *Physcomitrellopsis africana* genome assembly. The distribution shows two prominent peaks, with a smaller peak at ~7x coverage representing redundant haplotig sequences and a larger peak at ~65x representing the primary haploid genome coverage. The Purge Haplotigs pipeline used the local minima at 0x and 7x coverage as cutoffs to categorize and remove low coverage scaffolds presumed to be haplotigs or assembly artifacts. The 65x peak informed the coverage threshold for retaining the primary genome.

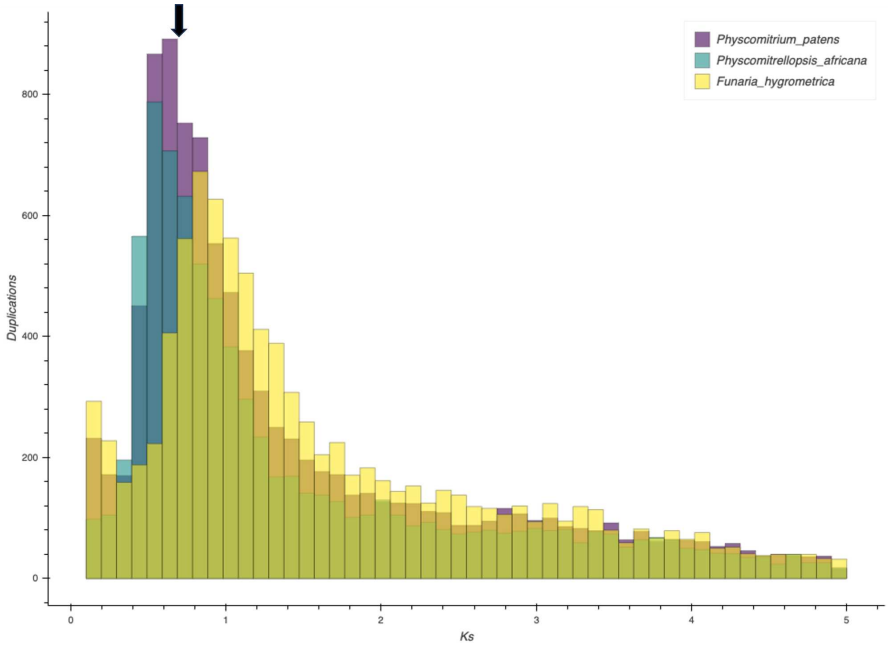

Fig S3: Ks density plots for *Physcomitrium patens*, *Funaria hygrometrica*, and *Physcomitrellopsis africana* genomes. Signatures of the two ancestral whole genome duplication (WGD) events are evident as shared peaks across all three species, as denoted by the black arrow. *Physcomitrium patens* exhibits a more prominent peak indicating greater retention of WGD duplicates compared to *Funaria hygrometrica* and *Physcomitrellopsis africana*.

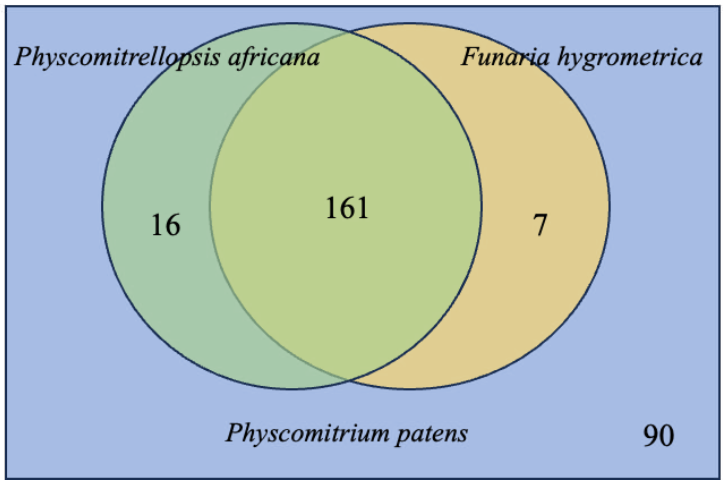

Fig. S4. Horizontally transferred genes (HGTs) identified in *Physcomitrium patens* assessed in both *Physcomitrellopsis africana* and *Funaria hygrometrica* genomes.

Literature Cited

Alboresi, A., Caffarri, S., Nogue, F., Bassi, R., & Morosinotto, T. (2008). In silico and biochemical analysis of Physcomitrella patens photosynthetic antenna: identification of subunits which evolved upon land adaptation. *PloS One*, *3*(4), e2033.

Altschul, S. F., Madden, T. L., Schäffer, A. A., Zhang, J., Zhang, Z., Miller, W., & Lipman, D. J. (1997). Gapped BLAST and PSI-BLAST: a new generation of protein database search programs. *Nucleic Acids Research*, *25*(17), 3389–3402.

Aminov, R. I. (2011). Horizontal gene exchange in environmental microbiota. *Frontiers in Microbiology*, *2*, 158.

Andrews, S. (2010). FastQC: a quality control tool for high throughput sequence data. Available online. *Retrieved May*, *17*, 2018.

Bechteler, J., Peñaloza-Bojacá, G., Bell, D., Burleigh, J. G., McDaniel, S. F., Christine Davis, E., Sessa, E. B., Bippus, A., Christine Cargill, D., Chantanoarrapint, S., Draper, I., Endara, L., Forrest, L. L., Garilleti, R., Graham, S. W., Huttunen, S., Jauregui Lazo, J., Lara, F., Larraín, J., … Villarreal A, J. C. (2023). Comprehensive phylogenomic time tree of bryophytes reveals deep relationships and uncovers gene incongruences in the last 500 million years of diversification. *American Journal of Botany*. https://doi.org/10.1002/ajb2.16249

Berg, G., Rybakova, D., Grube, M., & Köberl, M. (2016). The plant microbiome explored:

631 implications for experimental botany. *Journal of Experimental Botany*, *67*(4), 995–1002.
632 Boothby, T. C., Tenlen, J. R., Smith, F. W., Wang, J. R., Patanella, K. A., Nishimura, E. O.,
633 Tintori, S. C., Li, Q., Jones, C. D., Yandell, M., Messina, D. N., Glasscock, J., & Goldstein,
634 B. (2015). Evidence for extensive horizontal gene transfer from the draft genome of a
635 tardigrade. *Proceedings of the National Academy of Sciences of the United States of*
636 *America*, *112*(52), 15976–15981.
637 Brůna, T., Hoff, K. J., Lomsadze, A., Stanke, M., & Borodovsky, M. (2021). BRAKER2:
638 automatic eukaryotic genome annotation with GeneMark-EP+ and AUGUSTUS supported
639 by a protein database. *NAR Genomics and Bioinformatics*, *3*(1), lqaa108.
640 Buchfink, B., Reuter, K., & Drost, H.-G. (2021). Sensitive protein alignments at tree-of-life scale
641 using DIAMOND. *Nature Methods*, *18*(4), 366–368.
642 Caballero, M., & Wegrzyn, J. (2019). gFACs: Gene Filtering, Analysis, and Conversion to Unify
643 Genome Annotations Across Alignment and Gene Prediction Frameworks. *Genomics,*
644 *Proteomics & Bioinformatics*, *17*(3), 305–310.
645 Di Genova, A., Buena-Atienza, E., Ossowski, S., & Sagot, M.-F. (2021). Efficient hybrid de
646 novo assembly of human genomes with WENGAN. *Nature Biotechnology*, *39*(4), 422–430.
647 Douvlataniotis, K., Bensberg, M., Lentini, A., Gylemo, B., & Nestor, C. E. (2020). No evidence
648 for DNA N 6-methyladenine in mammals. *Science Advances*, *6*(12), eaay3335.
649 Emms, D. M., & Kelly, S. (2019). OrthoFinder: phylogenetic orthology inference for
650 comparative genomics. *Genome Biology*, *20*(1), 238.
651 Finn, R. D., Bateman, A., Clements, J., Coggill, P., Eberhardt, R. Y., Eddy, S. R., Heger, A.,
652 Hetherington, K., Holm, L., Mistry, J., Sonnhammer, E. L. L., Tate, J., & Punta, M. (2014).
653 Pfam: the protein families database. *Nucleic Acids Research*, *42*(Database issue), D222–
654 D230.
655 Flynn, J. M., Hubley, R., Goubert, C., Rosen, J., Clark, A. G., Feschotte, C., & Smit, A. F.
656 (2020). RepeatModeler2 for automated genomic discovery of transposable element families.
657 *Proceedings of the National Academy of Sciences of the United States of America*, *117*(17),
658 9451–9457.
659 Francois, C. M., Durand, F., Figuet, E., & Galtier, N. (2020). Prevalence and Implications of
660 Contamination in Public Genomic Resources: A Case Study of 43 Reference Arthropod
661 Assemblies. *G3*, *10*(2), 721–730.

662 Gabriel, L., Hoff, K. J., Brůna, T., Borodovsky, M., & Stanke, M. (2021). TSEBRA: transcript
663 selector for BRAKER. *BMC Bioinformatics*, *22*(1), 566.
664 Glime, J. M. (1990). The ecology column: Introduction. *The Bryological Times*, *55*, 5–7.
665 Grabherr, M. G., Haas, B. J., Yassour, M., Levin, J. Z., Thompson, D. A., Amit, I., Adiconis, X.,
666 Fan, L., Raychowdhury, R., Zeng, Q., Chen, Z., Mauceli, E., Hacohen, N., Gnirke, A.,
667 Rhind, N., di Palma, F., Birren, B. W., Nusbaum, C., Lindblad-Toh, K., … Regev, A.
668 (2011). Full-length transcriptome assembly from RNA-Seq data without a reference
669 genome. *Nature Biotechnology*, *29*(7), 644–652.
670 Guan, Y., Ma, L., Wang, Q., Zhao, J., Wang, S., Wu, J., Liu, Y., Sun, H., & Huang, J. (2023).
671 Horizontally acquired fungal killer protein genes affect cell development in mosses. *The*
672 *Plant Journal: For Cell and Molecular Biology*, *113*(4), 665–676.
673 Guo, X., Hu, X., Li, J., Shao, B., Wang, Y., Wang, L., Li, K., Lin, D., Wang, H., Gao, Z., Jiao,
674 Y., Wen, Y., Ji, H., Ma, C., Ge, S., Jiang, W., & Jin, X. (2023). The Sapria himalayana
675 genome provides new insights into the lifestyle of endoparasitic plants. *BMC Biology*,
676 *21*(1), 134.
677 Gurevich, A., Saveliev, V., Vyahhi, N., & Tesler, G. (2013). QUAST: quality assessment tool for
678 genome assemblies. *Bioinformatics*, *29*(8), 1072–1075.
679 Haas B, Papanicolaou A (2012) TransDecoder (Find Coding Regions within Transcripts)
680 [WWW Document]. https://transdecoder.github.io/.
681 Haghshenas, E., Asghari, H., Stoye, J., Chauve, C., & Hach, F. (2020). HASLR: Fast Hybrid
682 Assembly of Long Reads. *iScience*, *23*(8), 101389.
683 Haimlich, S., Fridman, Y., Khandal, H., Savaldi-Goldstein, S., & Levy, A. (2022). Widespread
684 horizontal gene transfer between plants and their microbiota. In *bioRxiv* (p.
685 2022.08.25.505314). https://doi.org/10.1101/2022.08.25.505314
686 Hart, A. J., Ginzburg, S., Xu, M. S., Fisher, C. R., Rahmatpour, N., Mitton, J. B., Paul, R., &
687 Wegrzyn, J. L. (2020). EnTAP: Bringing faster and smarter functional annotation to non-
688 model eukaryotic transcriptomes. *Molecular Ecology Resources*, *20*(2), 591–604.
689 Hornschuh, M., Grotha, R., & Kutschera, U. (2006). Moss-associated methylobacteria as
690 phytosymbionts: an experimental study. *Naturwissenschaften*, *93*(10), 480–486.
691 Huerta-Cepas, J., Szklarczyk, D., Heller, D., Hernández-Plaza, A., Forslund, S. K., Cook, H.,
692 Mende, D. R., Letunic, I., Rattei, T., Jensen, L. J., von Mering, C., & Bork, P. (2019).

eggNOG 5.0: a hierarchical, functionally and phylogenetically annotated orthology resource based on 5090 organisms and 2502 viruses. *Nucleic Acids Research*, *47*(D1), D309–D314.

Iwai, M., Grob, P., Iavarone, A. T., Nogales, E., & Niyogi, K. K. (2018). A unique supramolecular organization of photosystem I in the moss Physcomitrella patens. *Nature Plants*, *4*(11), 904–909.

Jones, P., Binns, D., Chang, H.-Y., Fraser, M., Li, W., McAnulla, C., McWilliam, H., Maslen, J., Mitchell, A., Nuka, G., Pesseat, S., Quinn, A. F., Sangrador-Vegas, A., Scheremetjew, M., Yong, S.-Y., Lopez, R., & Hunter, S. (2014). InterProScan 5: genome-scale protein function classification. *Bioinformatics*, *30*(9), 1236–1240.

Joshi NA, F. J. N. (2011). *Sickle: A sliding-window, adaptive, quality-based trimming tool for FastQ files* (Version Version 1.33). https://github.com/najoshi/sickle

Katoh, K., & Toh, H. (2008). Recent developments in the MAFFT multiple sequence alignment program. *Briefings in Bioinformatics*, *9*(4), 286–298.

Kim, D., Paggi, J. M., Park, C., Bennett, C., & Salzberg, S. L. (2019). Graph-based genome alignment and genotyping with HISAT2 and HISAT-genotype. *Nature Biotechnology*, *37*(8), 907–915.

Kim, D., Song, L., Breitwieser, F. P., & Salzberg, S. L. (2016). Centrifuge: rapid and sensitive classification of metagenomic sequences. *Genome Research*, *26*(12), 1721–1729.

Kirbis, A., Rahmatpour, N., Dong, S., Yu, J., van Gessel, N., Waller, M., Reski, R., Lang, D., Rensing, S. A., Temsch, E. M., Wegrzyn, J. L., Goffinet, B., Liu, Y., & Szövényi, P. (2022). Genome dynamics in mosses: Extensive synteny coexists with a highly dynamic gene space. In *bioRxiv* (p. 2022.05.17.492078). https://doi.org/10.1101/2022.05.17.492078

Kirbis, A., Waller, M., Ricca, M., Bont, Z., Neubauer, A., Goffinet, B., & Szövényi, P. (2020). Transcriptional landscapes of divergent sporophyte development in two mosses, Physcomitrium (Physcomitrella) patens and Funaria hygrometrica. *Frontiers in Plant Science*, *11*, 747.

Kirsch, R., Okamura, Y., Haeger, W., Vogel, H., Kunert, G., & Pauchet, Y. (2022). Metabolic novelty originating from horizontal gene transfer is essential for leaf beetle survival. *Proceedings of the National Academy of Sciences of the United States of America*, *119*(40), e2205857119.

Kolmogorov, M., Yuan, J., Lin, Y., & Pevzner, P. A. (2019). Assembly of long, error-prone

reads using repeat graphs. *Nature Biotechnology*, *37*(5), 540–546.

Koutsovoulos, G., Kumar, S., Laetsch, D. R., Stevens, L., Daub, J., Conlon, C., Maroon, H., Thomas, F., Aboobaker, A. A., & Blaxter, M. (2016). No evidence for extensive horizontal gene transfer in the genome of the tardigrade Hypsibius dujardini [Review of *No evidence for extensive horizontal gene transfer in the genome of the tardigrade Hypsibius dujardini*]. *Proceedings of the National Academy of Sciences of the United States of America*, *113*(18), 5053–5058.

Kovaka, S., Zimin, A. V., Pertea, G. M., Razaghi, R., Salzberg, S. L., & Pertea, M. (2019). Transcriptome assembly from long-read RNA-seq alignments with StringTie2. *Genome Biology*, *20*(1), 278.

Lang, D., Ullrich, K. K., Murat, F., Fuchs, J., Jenkins, J., Haas, F. B., Piednoel, M., Gundlach, H., Van Bel, M., Meyberg, R., Vives, C., Morata, J., Symeonidi, A., Hiss, M., Muchero, W., Kamisugi, Y., Saleh, O., Blanc, G., Decker, E. L., … Rensing, S. A. (2018). The Physcomitrella patens chromosome-scale assembly reveals moss genome structure and evolution. *The Plant Journal*, *93*(3), 515–533.

Li, B., & Dewey, C. N. (2011). RSEM: accurate transcript quantification from RNA-Seq data with or without a reference genome. *BMC Bioinformatics*, *12*, 323.

Li, F.-W., Brouwer, P., Carretero-Paulet, L., Cheng, S., de Vries, J., Delaux, P.-M., Eily, A., Koppers, N., Kuo, L.-Y., Li, Z., Simenc, M., Small, I., Wafula, E., Angarita, S., Barker, M. S., Bräutigam, A., dePamphilis, C., Gould, S., Hosmani, P. S., … Pryer, K. M. (2018). Fern genomes elucidate land plant evolution and cyanobacterial symbioses. *Nature Plants*, *4*(7), 460–472.

Ma, J., Wang, S., Zhu, X., Sun, G., Chang, G., Li, L., Hu, X., Zhang, S., Zhou, Y., Song, C.-P., & Huang, J. (2022). Major episodes of horizontal gene transfer drove the evolution of land plants. *Molecular Plant*, *15*(5), 857–871.

Manni, M., Berkeley, M. R., Seppey, M., & Zdobnov, E. M. (2021). BUSCO: Assessing Genomic Data Quality and Beyond. *Current Protocols*, *1*(12), e323.

Marçais, G., & Kingsford, C. (2011). A fast, lock-free approach for efficient parallel counting of occurrences of k-mers. *Bioinformatics*, *27*(6), 764–770.

Martin, F. M., Uroz, S., & Barker, D. G. (2017). Ancestral alliances: Plant mutualistic symbioses with fungi and bacteria. *Science*, *356*(6340), ea.ad4501

https://doi.org/10.1126/science.aad4501

Medina, R., Johnson, M., Liu, Y., Wilding, N., Hedderson, T. A., Wickett, N., & Goffinet, B. (2018). Evolutionary dynamism in bryophytes: Phylogenomic inferences confirm rapid radiation in the moss family Funariaceae. *Molecular Phylogenetics and Evolution*, *120*, 240–247.

Medina, R., M. G. Johnson, Y. Liu, N.J. Wickett, A.J. Shaw & B. Goffinet. 2019. Phylogenomic delineation of Physcomitrium (Bryophyta: Funariaceae) based on nuclear targeted exons and their flanking regions rejects the retention of Physcomitrella, Physcomitridium and Aphanorrhegma. *Journal of Systematics and Evolution, 57*, 404–417.Price, M. N., Dehal, P. S., & Arkin, A. P. (2010). FastTree 2 – Approximately Maximum-Likelihood Trees for Large Alignments. *PloS One*, *5*(3), e9490.

Proost, S., Fostier, J., De Witte, D., Dhoedt, B., Demeester, P., Van de Peer, Y., & Vandepoele, K. (2011). i-ADHoRe 3.0—fast and sensitive detection of genomic homology in extremely large data sets. *Nucleic Acids Research*, *40*(2), e11–e11.

Rahmatpour, N., Perera, N. V., Singh, V., Wegrzyn, J. L., & Goffinet, B. (2021). High gene space divergence contrasts with frozen vegetative architecture in the moss family Funariaceae. *Molecular Phylogenetics and Evolution*, *154*, 106965.

Ranallo-Benavidez, T. R., Jaron, K. S., & Schatz, M. C. (2020). GenomeScope 2.0 and Smudgeplot for reference-free profiling of polyploid genomes. *Nature Communications*, *11*(1), 1432.

Rensing, S. A., Goffinet, B., Meyberg, R., Wu, S.-Z., & Bezanilla, M. (2020). The moss Physcomitrium (Physcomitrella) patens: A model organism for non-seed plants. *The Plant Cell*, *32*(5), 1361–1376.

Rensing, S. A., Lang, D., Zimmer, A. D., Terry, A., Salamov, A., Shapiro, H., Nishiyama, T., Perroud, P.-F., Lindquist, E. A., Kamisugi, Y., Tanahashi, T., Sakakibara, K., Fujita, T., Oishi, K., Shin-I, T., Kuroki, Y., Toyoda, A., Suzuki, Y., Hashimoto, S.-I., … Boore, J. L. (2008). The Physcomitrella genome reveals evolutionary insights into the conquest of land by plants. *Science*, *319*(5859), 64–69.

Rhie, A., Walenz, B. P., Koren, S., & Phillippy, A. M. (2020). Merqury: reference-free quality, completeness, and phasing assessment for genome assemblies. *Genome Biology*, *21*(1), 245.

Roach, M. J., Schmidt, S. A., & Borneman, A. R. (2018). Purge Haplotigs: allelic contig

786 reassignment for third-gen diploid genome assemblies. *BMC Bioinformatics*, *19*(1), 460.
787 Smit, AFA, Hubley, R & Green, P. (2013-2015). *RepeatMasker Open-4.0*. RepearMasker.
788 http://www.repeatmasker.org
789 Sun, G., Bai, S., Guan, Y., Wang, S., Wang, Q., Liu, Y., Liu, H., Goffinet, B., Zhou, Y., Paoletti,
790 M., Hu, X., Haas, F. B., Fernandez-Pozo, N., Czyrt, A., Sun, H., Rensing, S. A., & Huang,
791 J. (2020). Are fungi-derived genomic regions related to antagonism towards fungi in
792 mosses? *The New Phytologist*, *228*(4), 1169–1175.
793 Sun, H., Shang, H., Pan, X., & Li, M. (2023). Structural insights into the assembly and energy
794 transfer of the Lhcb9-dependent photosystem I from moss Physcomitrium patens. *Nature*
795 *Plants*, *9*(8), 1347–1358.
796 Van Dongen, S. M. (2000). Graph clustering by flow simulation. Doctoral dissertation. Utrecht
797 University, Netherlands.
798 Van Etten, J., & Bhattacharya, D. (2020). Horizontal gene transfer in Eukaryotes: Not if, but how
799 much? *Trends in Genetics*, *36*(12), 915–925.
800 Vuruputoor, V. S., Monyak, D., Fetter, K. C., Webster, C., Bhattarai, A., Shrestha, B., Zaman,
801 S., Bennett, J., McEvoy, S. L., Caballero, M., & Wegrzyn, J. L. (2022). Welcome to the big
802 leaves: best practices for improving genome annotation in non-model plant genomes. In
803 *bioRxiv* (p. 2022.10.03.510643). https://doi.org/10.1101/2022.10.03.510643
804 Walker, B. J., Abeel, T., Shea, T., Priest, M., Abouelliel, A., Sakthikumar, S., Cuomo, C. A.,
805 Zeng, Q., Wortman, J., Young, S. K., & Earl, A. M. (2014). Pilon: an integrated tool for
806 comprehensive microbial variant detection and genome assembly improvement. *PloS One*,
807 *9*(11), e112963.
808 Wang, S., Guan, Y., Wang, Q., Zhao, J., Sun, G., Hu, X., Running, M. P., Sun, H., & Huang, J.
809 (2020). A mycorrhizae-like gene regulates stem cell and gametophore development in
810 mosses. *Nature Communications*, *11*(1), 2030.
811 Wilding, N. (2015). Systematics, biogeography and morphological evolution in Entosthodon
812 Schwägr. (Bryopsida, Funariaceae) with a revision of the genus in Africa. Doctoral
813 dissertation. University of Cape Town, South Africa.
814 Xi, Z., Bradley, R. K., Wurdack, K. J., Wong, K., Sugumaran, M., Bomblies, K., Rest, J. S., &
815 Davis, C. C. (2012). Horizontal transfer of expressed genes in a parasitic flowering plant.
816 *BMC Genomics*, *13*, 227.

817 Yang, Z. (2007). PAML 4: Phylogenetic Analysis by Maximum Likelihood. *Molecular Biology*
818 *and Evolution*, *24*(8), 1586–1591.
819 Young, M. D., Wakefield, M. J., Smyth, G. K., & Oshlack, A. (2010). Gene ontology analysis
820 for RNA-seq: accounting for selection bias. *Genome Biology*, *11*(2), R14.
821 Young, LA, (2022). *Relationships Among AA-Genome Chenopodium Diploids and a Whole*
822 *Genome Assembly of the North American Species, C. watsonii* (Doctoral dissertation,
823 Brigham Young University)
824 Yu, J., Li, L., Wang, S., Dong, S., Chen, Z., Patel, N., Goffinet, B., Chen, H., Liu, H., & Liu, Y.
825 (2020). Draft genome of the aquatic moss Fontinalis antipyretica (Fontinalaceae,
826 Bryophyta). *GigaByte*, *2020*, gigabyte8.
827 Zhang, J., Fu, X.-X., Li, R.-Q., Zhao, X., Liu, Y., Li, M.-H., Zwaenepoel, A., Ma, H., Goffinet,
828 B., Guan, Y.-L., Xue, J.-Y., Liao, Y.-Y., Wang, Q.-F., Wang, Q.-H., Wang, J.-Y., Zhang,
829 G.-Q., Wang, Z.-W., Jia, Y., Wang, M.-Z., … Chen, Z.-D. (2020). The hornwort genome
830 and early land plant evolution. *Nature Plants*, *6*(2), 107–118.
831 Zhang, Z., & Wood, W. I. (2003). A profile hidden Markov model for signal peptides generated
832 by HMMER. *Bioinformatics*, *19*(2), 307–308.
833 Zimin, A. V., Marçais, G., Puiu, D., Roberts, M., Salzberg, S. L., & Yorke, J. A. (2013). The
834 MaSuRCA genome assembler. *Bioinformatics*, *29*(21), 2669–2677.
835 Zimmer, A. D., Lang, D., Buchta, K., Rombauts, S., Nishiyama, T., Hasebe, M., ... & Reski, R.
836 (2013). Reannotation and extended community resources for the genome of the non-seed
837 plant Physcomitrella patens provide insights into the evolution of plant gene structures and
838 functions. *BMC Genomics*, *14*, 1–20.
839 Zwaenepoel, A., & Van de Peer, Y. (2018). wgd—simple command line tools for the analysis of
840 ancient whole-genome duplications. *Bioinformatics*, *35*(12), 2153–2155.


A

B

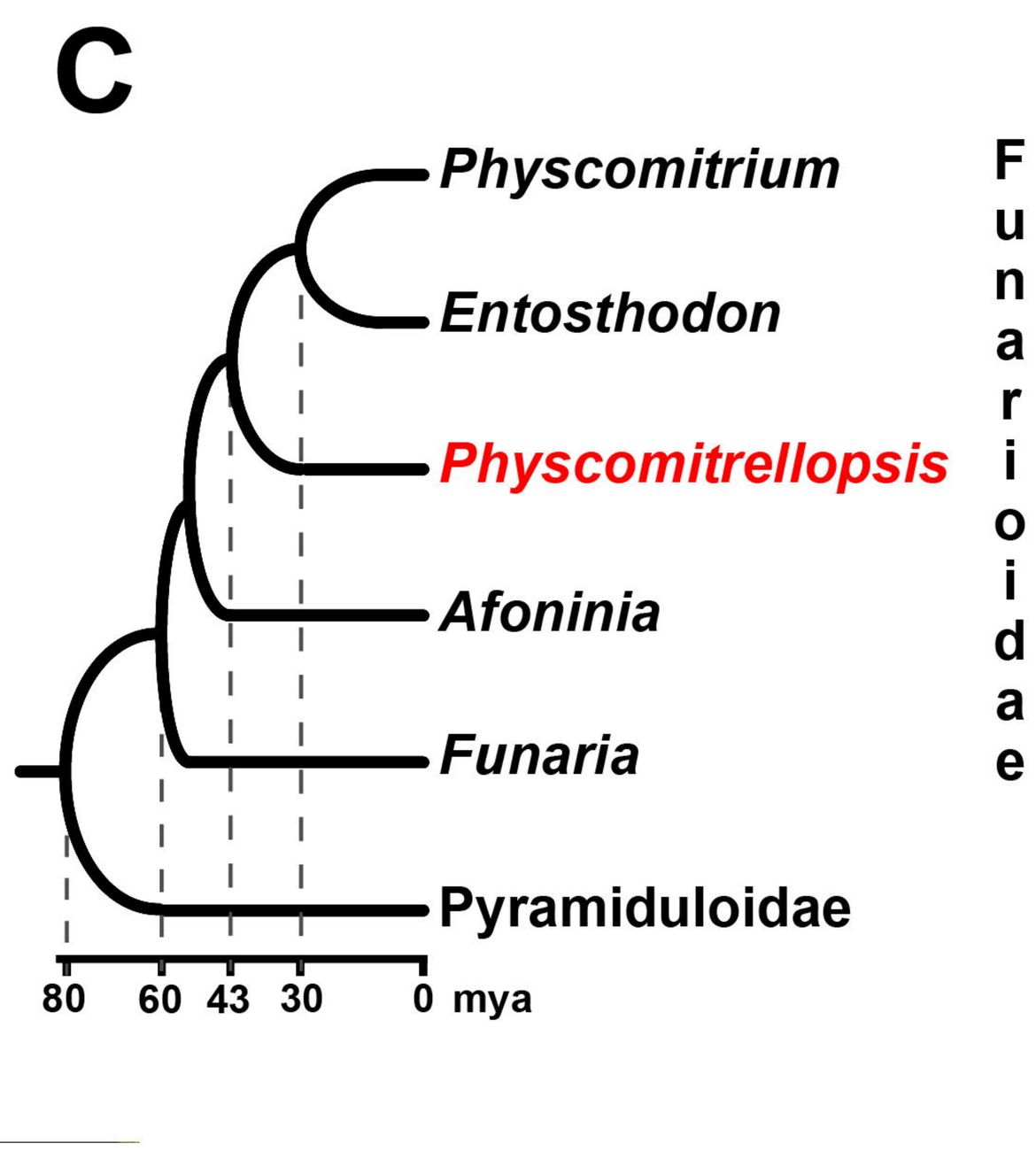
C
Physcomitrium
Entosthodon
Physcomitrellopsis
Afoninia
Funaria
Pyramiduloidae
80
60
43
30
0 mya
Funarioidae

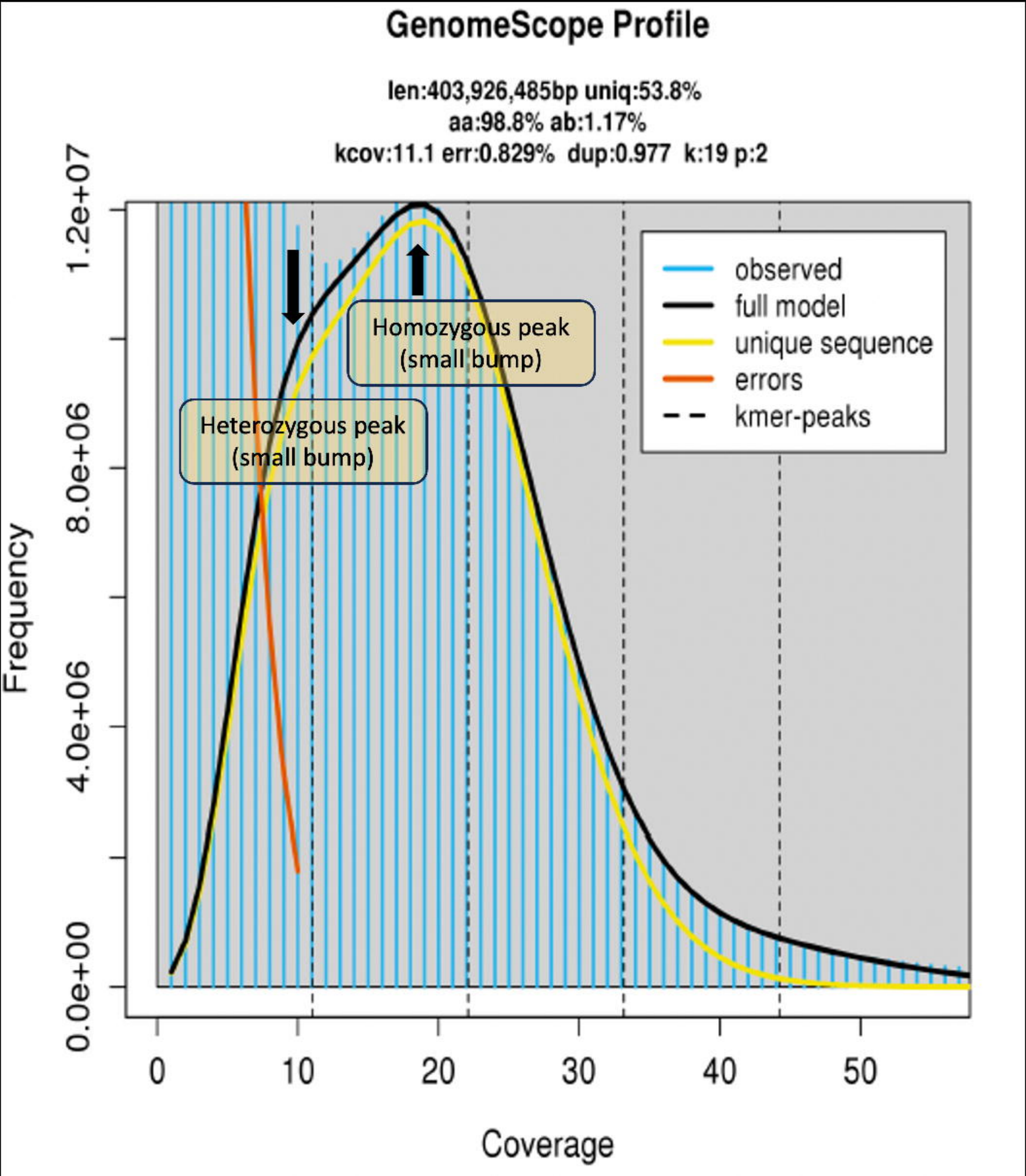
GenomeScope Profile
len:403,926,485bp uniq:53.8%
aa:98.8% ab:1.17%
kcov:11.1 err:0.829% dup:0.977 k:19 p:2
observed
full model
unique sequence
errors
kmer-peaks
Homozygous peak
(small bump)
Heterozygous peak
(small bump)
Frequency
0.0e+00
4.0e+06
8.0e+06
1.2e+07
0
10
20
30
40
50
Coverage

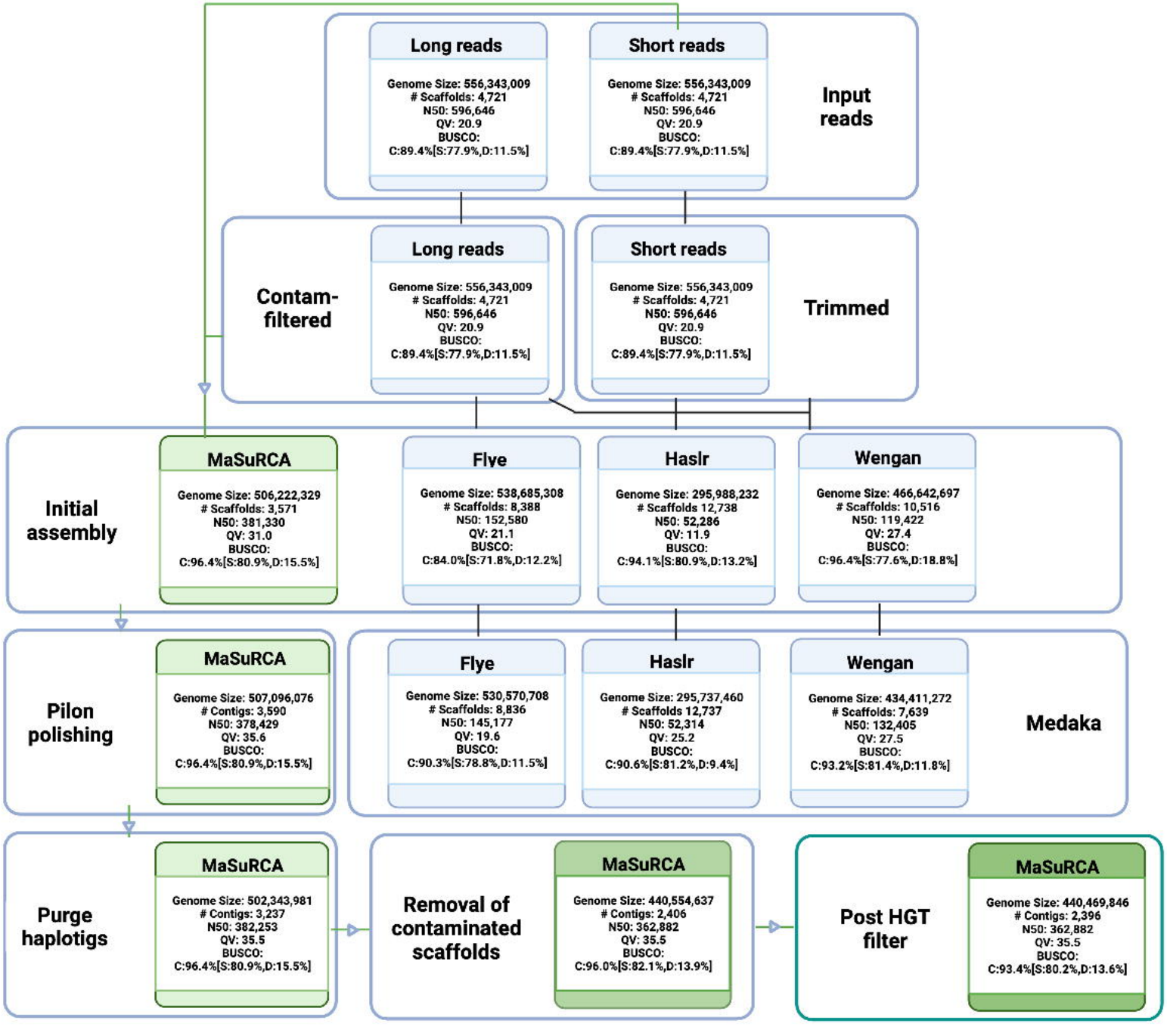
Long reads
Genome Size: 556,343,009
Scaffolds: 4,721
N50: 596,646
QV: 20.9
BUSCO:
C:89.4%[S:77.9%,D:11.5%]
Short reads
Genome Size: 556,343,009
Scaffolds: 4,721
N50: 596,646
QV: 20.9
BUSCO:
C:89.4%[S:77.9%,D:11.5%]
Input reads
Contam-filtered
Long reads
Genome Size: 556,343,009
Scaffolds: 4,721
N50: 596,646
QV: 20.9
BUSCO:
C:89.4%[S:77.9%,D:11.5%]
Short reads
Genome Size: 556,343,009
Scaffolds: 4,721
N50: 596,646
QV: 20.9
BUSCO:
C:89.4%[S:77.9%,D:11.5%]
Trimmed
Initial assembly
MaSuRCA
Genome Size: 506,222,329
Scaffolds: 3,571
N50: 381,330
QV: 31.0
BUSCO:
C:96.4%[S:80.9%,D:15.5%]
Flye
Genome Size: 538,685,308
Scaffolds: 8,388
N50: 152,580
QV: 21.1
BUSCO:
C:84.0%[S:71.8%,D:12.2%]
Haslr
Genome Size: 295,988,232
Scaffolds 12,738
N50: 52,286
QV: 11.9
BUSCO:
C:94.1%[S:80.9%,D:13.2%]
Wengan
Genome Size: 466,642,697
Scaffolds: 10,516
N50: 119,422
QV: 27.4
BUSCO:
C:96.4%[S:77.6%,D:18.8%]
Pilon polishing
MaSuRCA
Genome Size: 507,096,076
Contigs: 3,590
N50: 378,429
QV: 35.6
BUSCO:
C:96.4%[S:80.9%,D:15.5%]
Flye
Genome Size: 530,570,708
Scaffolds: 8,836
N50: 145,177
QV: 19.6
BUSCO:
C:90.3%[S:78.8%,D:11.5%]
Haslr
Genome Size: 295,737,460
Scaffolds 12,737
N50: 52,314
QV: 25.2
BUSCO:
C:90.6%[S:81.2%,D:9.4%]
Wengan
Genome Size: 434,411,272
Scaffolds: 7,639
N50: 132,405
QV: 27.5
BUSCO:
C:93.2%[S:81.4%,D:11.8%]
Medaka
Purge haplotigs
MaSuRCA
Genome Size: 502,343,981
Contigs: 3,237
N50: 382,253
QV: 35.5
BUSCO:
C:96.4%[S:80.9%,D:15.5%]
Removal of contaminated scaffolds
MaSuRCA
Genome Size: 440,554,637
Contigs: 2,406
N50: 362,882
QV: 35.5
BUSCO:
C:96.0%[S:82.1%,D:13.9%]
Post HGT filter
MaSuRCA
Genome Size: 440,469,846
Contigs: 2,396
N50: 362,882
QV: 35.5
BUSCO:
C:93.4%[S:80.2%,D:13.6%]

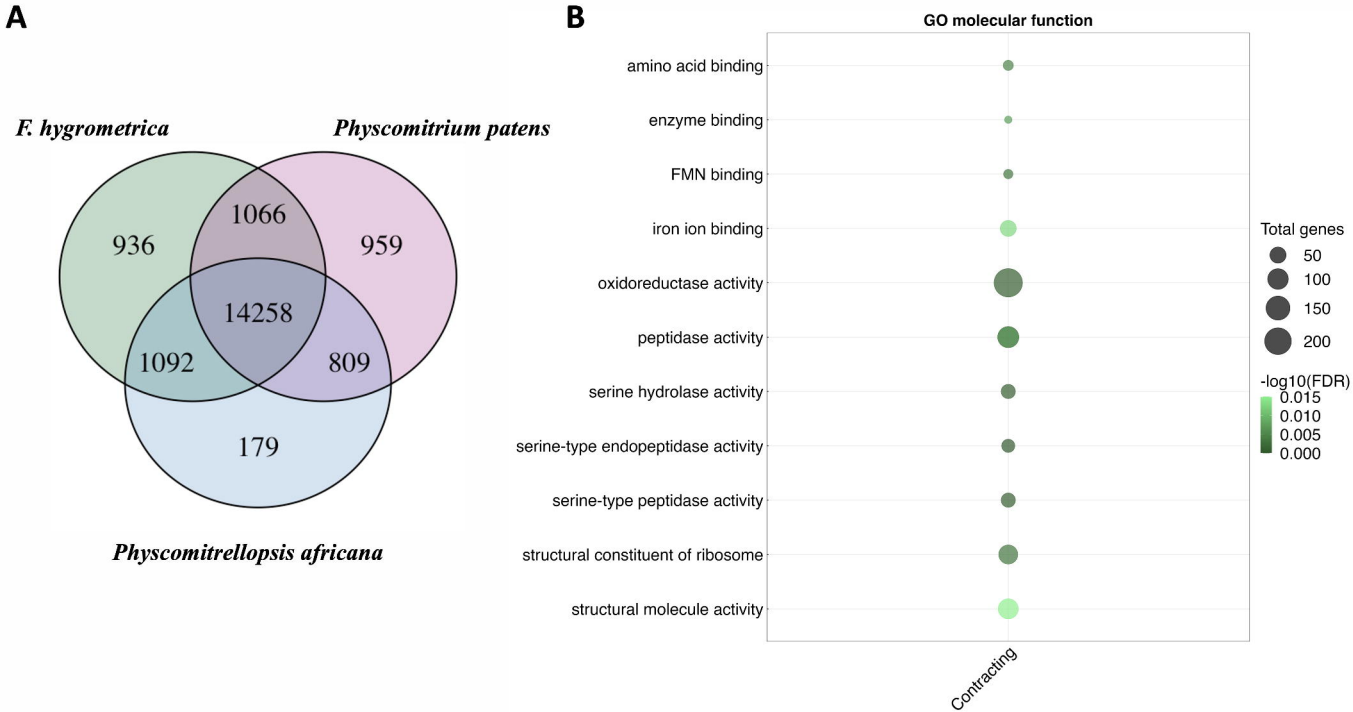
A
F. hygrometrica
Physcomitrium patens
936
1066
959
14258
1092
809
179
Physcomitrellopsis africana
B
GO molecular function
amino acid binding
enzyme binding
FMN binding
iron ion binding
oxidoreductase activity
peptidase activity
serine hydrolase activity
serine-type endopeptidase activity
serine-type peptidase activity
structural constituent of ribosome
structural molecule activity
Contracting
Total genes
50
100
150
200
-log10(FDR)
0.015
0.010
0.005
0.000


A
scaffold_0062:414,417-424,781
10 kb
416 kb
418 kb
420 kb
422 kb
424 kb
Annotation GTF of Physcomitrellopsis africana
StringTie2 transcripts
Alignment of NR hits to the genome
Alignment of P. patens proteins to the genome
Alignment of C. purpureus proteins to the genome
Pa1_04827.1
Pa1_04828
Pa1_04829
STRG.5308
STRG.5310
WP_207424935.1
MP000780
MP000461
MP000436
B
scaffold_1363:26,806-40,495
13 kb
28 kb
30 kb
32 kb
34 kb
36 kb
38 kb
40 kb
Pa1_22335.1
Pa1_22336.1
Pa1_22337.1
STRG.24351
STRG.24354
MCB2107078.1
MP001460
MP001273
MP000247
MP000355
MP000186
C
scaffold_0465:130,600-154,988
24 kb
132 kb
134 kb
136 kb
138 kb
140 kb
142 kb
144 kb
146 kb
148 kb
150 kb
152 kb
154 kb
Pa1_15636.1
MP000002

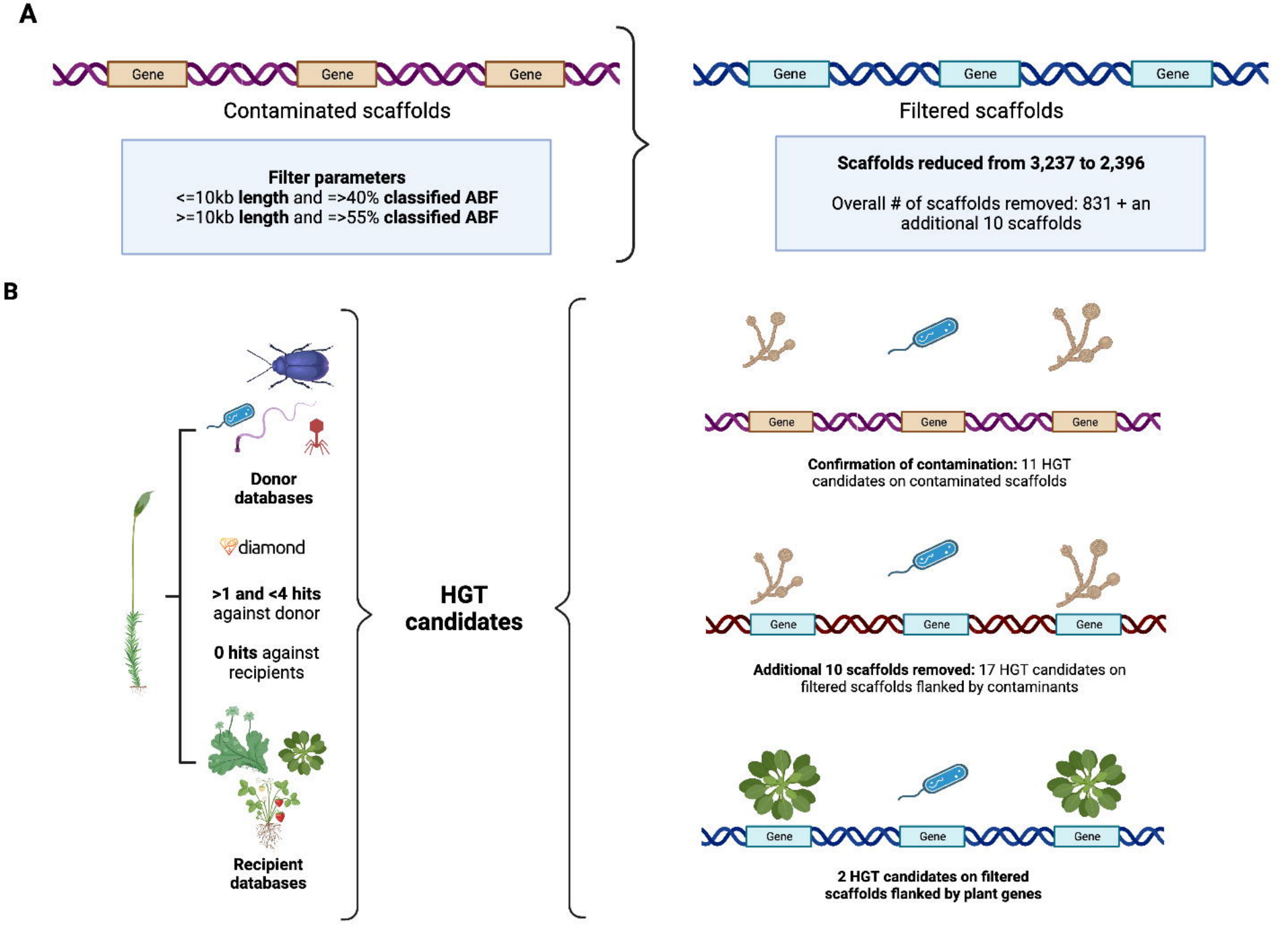
A
Gene
Gene
Gene
Contaminated scaffolds
Filter parameters
<=10kb length and =>40% classified ABF
>=10kb length and =>55% classified ABF
Gene
Gene
Gene
Filtered scaffolds
Scaffolds reduced from 3,237 to 2,396
Overall # of scaffolds removed: 831 + an additional 10 scaffolds
B
Donor databases
diamond
>1 and <4 hits against donor
0 hits against recipients
Recipient databases
HGT candidates
Gene
Gene
Gene
Confirmation of contamination: 11 HGT candidates on contaminated scaffolds
Gene
Gene
Gene
Additional 10 scaffolds removed: 17 HGT candidates on filtered scaffolds flanked by contaminants
Gene
Gene
Gene
2 HGT candidates on filtered scaffolds flanked by plant genes

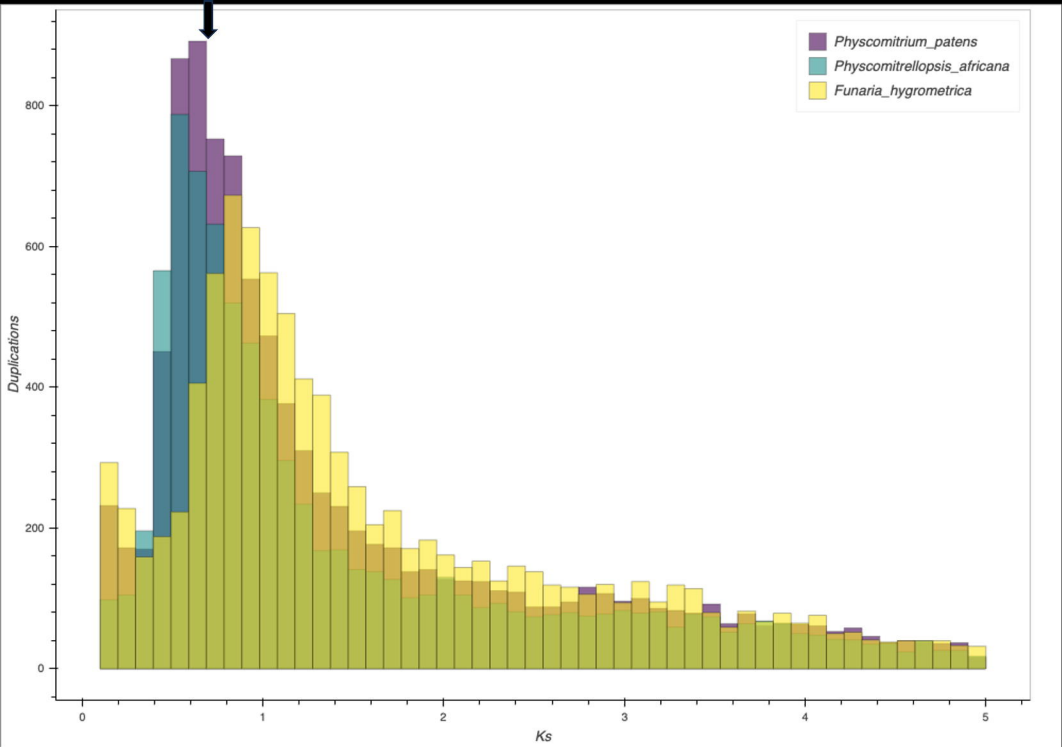
Physcomitrium_patens
Physcomitrellopsis_africana
Funaria_hygrometrica
Duplications
800
600
400
200
0
0
1
2
3
4
5
Ks

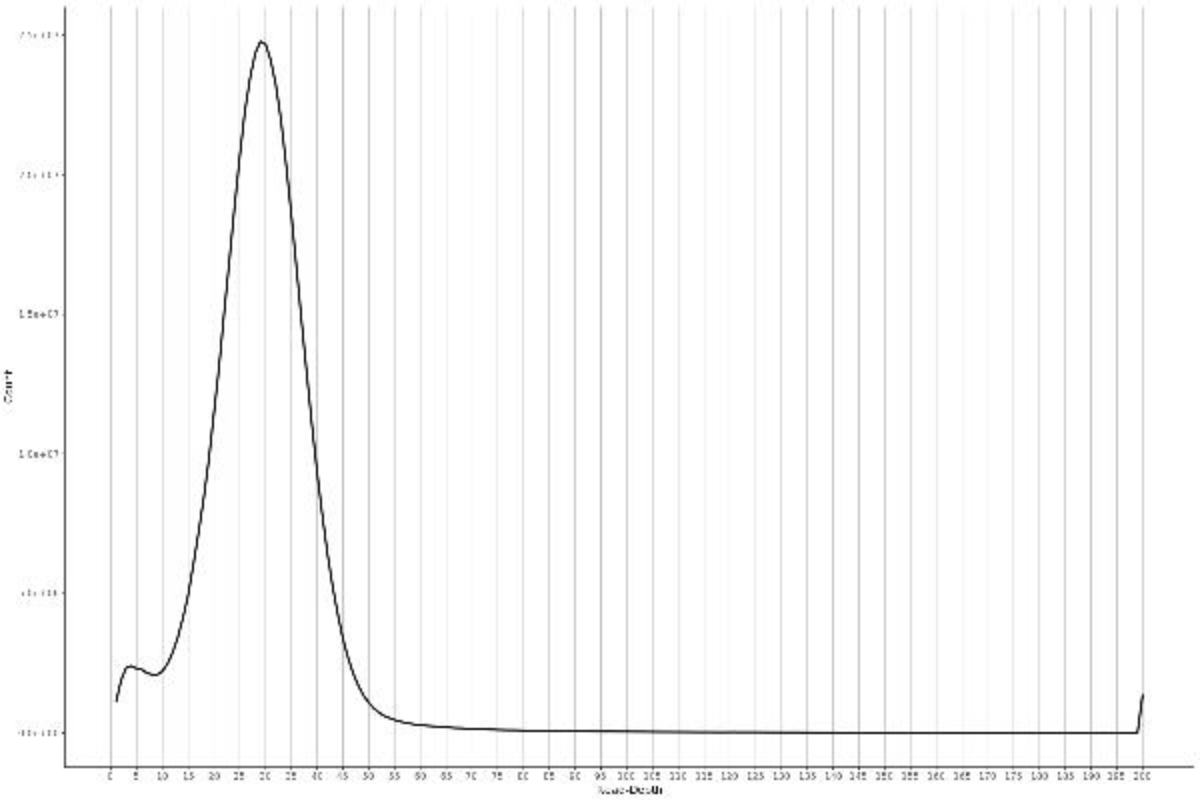
Count
1.0e+07
5.0e+06
0
5
10
15
20
25
30
35
40
45
50
55
60
65
70
75
80
85
90
95
100
105
110
115
120
125
130
135
140
145
150
155
160
165
170
175
180
185
190
195
200